# Dendritic voltage imaging reveals biophysical basis of associative plasticity rules

Pojeong Park[1]*, David Wong-Campos[1]*, Daniel G. Itkis[1], Yitong Qi[1], Hunter Davis[1], Jonathan B. Grimm[2], Sarah E. Plutkis[2], Luke Lavis[2], Adam E. Cohen[1,3]

[1]Department of Chemistry and Chemical Biology, Harvard University, Cambridge, MA, USA
[2]Janelia Research Campus, Howard Hughes Medical Institute, Ashburn, Virginia, USA
[3]Department of Physics, Harvard University, Cambridge, MA, USA

* Equal contribution
contact: cohen@chemistry.harvard.edu

## Abstract

Dendrites on neurons integrate synaptic inputs to determine spike timing. Dendrites also convey back-propagating action potentials (bAPs), where these signals interact with synaptic inputs to strengthen or weaken individual synapses. To study dendritic integration and associative plasticity rules, we developed molecular, optical, and computational tools for all-optical electrophysiology in dendrites. We mapped sub-millisecond voltage dynamics throughout the dendritic trees of CA1 pyramidal neurons in acute brain slices. Our data show history-dependent bAP propagation in distal dendrites, driven by locally generated $Na^+$ spikes (dSpikes). Dendritic depolarization led to a transient window for dSpike propagation, opened by A-type $K_V$ channel inactivation, and closed by slow $Na_V$ inactivation. Collisions of dSpikes with synaptic inputs triggered N-methyl-D-aspartate receptor (NMDAR)-dependent plateau potentials. These results, combined with numerical simulations, paint an intuitive picture connecting dendritic biophysics to associative plasticity rules.

Dendrites carry information in two directions: they integrate synaptic inputs to determine spike times at the soma, and they combine back-propagating action potentials with synaptic inputs to mediate changes in synaptic strength.[1–3] Electrical signals propagating in either direction encounter a diverse set of ion channels which give the dendrite nonlinear and history-dependent excitability. How do dendrites carry out the distinct tasks of dendritic integration and spike back propagation with a single set of excitability rules? More generally, what is the relation between dendritic biophysics and bidirectional dendritic information processing?

Dendrites exhibit many nonlinearities and distinct regenerative excitations, such as sodium[4,5], calcium[6,7], and NMDA[8–10] spikes. While these events have been characterized in detail,[11–14] their functional significance remains unclear. Inconsistent reports about the basic phenomenology of bAP propagation complicate the picture. Trains of bAPs in pyramidal neurons have been reported to exhibit facilitation (successive increases in amplitude in distal dendrites)[15], depression (successive decreases)[16], or stochastic propagation[17]. It has not been clear what variables govern these different activity patterns. To understand information flow and processing in dendrites, one would like to inject signals in arbitrary patterns of space and time and to record the resulting voltage dynamics throughout the dendritic tree.

We developed tools to perturb and measure voltage throughout dendritic trees by combining targeted optogenetic stimulation, fluorescent voltage indicators, and structured illumination microscopy (Fig. 1). We modified a blue-shifted channelrhodopsin, CheRiff[18], and a chemigenetic voltage indicator, Voltron2[19], to improve dendritic expression by attaching an N-terminal Lucy-Rho tag[20] and C-terminal ER export and TS trafficking motifs[21,22]. We expressed both constructs from a bicistronic vector in mouse hippocampal CA1 pyramidal neurons, and then prepared acute brain slices (Methods). First, we made high-resolution structural images via 2-photon (2P) microscopy. Next, we combined micromirror-patterned optogenetic stimulation with structured illumination high-speed (1 kHz) voltage imaging (Fig. 1a-b). Finally, the structural and functional data were fused to make high spatiotemporal resolution maps showing the amplitude and timing of spike back-propagation (Fig. 1c-e, S1, Methods). Sub-Nyquist interpolation of action potential upstrokes[18] revealed details of bAP wavefront motion with 25 μs time resolution (Fig. 1f, Methods). This system allowed us to probe the fine-grained bioelectrical responses to arbitrary spatiotemporal patterns of stimulation.

**Distal dendritic depolarization favors dendritic spikes (dSpikes)**

We sequentially stimulated different dendritic branches and mapped the bioelectrical responses. We asked: 1) Do localized stimuli evoke local dendritic excitations or other signs of nonlinear dendritic integration? 2) Does the location of the stimulus affect the

spatial profile of the bAP, i.e. do bAPs know where they were born? And 3) Does the voltage history affect bAP propagation, i.e. do bAPs know about their past?

Optogenetic stimuli (20 ms duration, 5 Hz, 54 repeats) were delivered either to one of several dendritic branches (Fig. 2a-f, Fig. S2), the soma (Fig. 2g), or the soma and a distal dendrite (Fig. 2h). The stimuli generated subthreshold depolarizations (Fig. 2a) and then bursts of 2 – 3 spikes. Experiments were repeated in $n$ = 17 neurons from 15 animals. We noted several consistent features of the dendritic voltage responses:

First, the subthreshold voltage profile moved with the stimulus location: depolarization was largest in the stimulated branch and decayed smoothly outward, as expected for passive cable propagation. We never observed spikes or plateau potentials that initiated in the dendrites (Fig. S4). Dendritic integration appeared to be dominated by passive cable properties.

Second, spikes always initiated at the soma, regardless of stimulus location, and then propagated back into the dendritic tree (our experiments did not resolve the axon or axon initial segment). All spikes had similar waveforms at the soma, but the waveforms at distal dendrites revealed distinct bAP propagation motifs (Fig. 2d). In some trials, the voltage in the distal dendrites appeared as a low-pass-filtered version of the somatic voltage, indicative of bAP attenuation. In other trials, the distal dendrites showed a single qualitatively distinct spike. We called these events “dendritic spikes” or dSpikes.

For each stimulus location, we classified stimulus trials into those without or with a dSpike, and for each class we calculated spatial profiles and kymographs of the bAP propagation along the main apical dendrite (Fig. 2b,c,f,g, Fig. S3, Methods).

DSpikes always arose from a growing bAP, never on their own. Remarkably, bAPs and dSpikes each had stereotyped spatial profiles that were consistent across trials and stimulus locations (Fig. S4). bAPs reliably engaged all perisomatic and proximal dendrites and failed along the distal trunk, while dSpikes reliably engaged all distal dendrites too. The amplitude of dSpikes relative to the first bAP (i.e., $\Delta F_{max}/\Delta F_1$) was maximum in the distal dendritic trunk (313 ± 41 µm, mean ± s.d., $n$ = 22 stimulated regions (soma or proximal branch), 17 neurons, 15 animals; Fig. 2i,j). Thus, in these experiments, the neurons produced precisely two kinds of excitations in apical dendrites: perisomatic bAPs and distal dSpikes—and neither spatial profile was sensitive to the location of the driving stimulus.

Third, the probability that a bAP became a dSpike depended on the stimulus location and depolarization history of the distal dendrites. Distal stimuli (> 250 µm from the soma)

reliably evoked dSpikes on the first bAP, while proximal stimuli (< 200 μm from the soma) almost never evoked dSpikes on the first bAP, but sometimes evoked dSpikes on the second or third bAP (Fig. 2k). Pooled data from 35 branch stimulations (*n* = 13 cells from 11 animals) revealed that the probability of evoking a dSpike with the first bAP followed a sigmoidal distance dependence, with a plateau of ~80% success rate for stimuli > 300 μm from the soma (Fig. 2k).

These seemingly complex dSpike dynamics could be described with a simple rule. dSpikes arose if and only if the distal dendrites had been depolarized for at least 15 ms prior to arrival of a bAP (Fig. 2e-h). Distal stimuli took approximately 15 ms to depolarize the soma enough to elicit a spike. As a result, stimulation at a distal dendrite (e.g., D2) produced dSpikes on the first bAP in most cases (Fig. 2f). In contrast, stimuli at the soma or proximal dendrites began evoking rapid somatic spikes before the distal dendrites were depolarized. These bAPs failed to produce dSpikes, but they contributed to depolarizing the distal dendrites, opening a window for dSpike formation from subsequent bAPs.

This rule is illustrated by comparing Figs. 2f, g, and h. Stimulation of distal dendrite D2 alone evoked dSpikes on the first bAP, with 65% probability (35 of 54 trials). These bAPs came 15 – 20 ms after stimulus onset, due to the time required for the distal stimulus to depolarize the soma enough to evoke a first spike. Stimulation of the soma alone never evoked dSpikes on the first two bAPs, and occasionally evoked a dSpike on the third bAP (6 of 54 trials), which came 13 – 17 ms after stimulus onset. Simultaneous stimulation at soma and D2 produced two quick bAPs which failed to evoke dSpikes, and then the third bAP (15 – 17 ms after stimulus onset) triggered a dSpike with 100% probability (Fig. 2h).

Prior work had suggested that a critical spike rate needed to be exceeded to evoke dendritic spikes.[15,23] Our results show that the somatic spike rate is not the key variable, but rather the dendritic depolarization. An isolated bAP can become a dSpike if the distal dendrites are pre-depolarized; but if the main excitatory input is at or near the soma, a current large enough to depolarize the distal dendrites also, incidentally, produces a high spike rate at the soma.

**Dendritic spike time-window in distal dendrites**

Sustained optogenetic stimuli (> 200 ms duration) evoked a biphasic pattern of bAP propagation. For example, a sustained stimulus to a proximal apical dendrite evoked a bAP without a dSpike, then two bAPs with dSpikes, then a series of bAPs without dSpikes (Fig. 3a). Pooled data (*n* = 43 stimulated branches, 16 cells, 13 animals) showed that upon onset of optogenetic stimulation, dSpikes failed for the first 18 ± 7 ms (mean ± s.d.), then there was a period where dSpikes succeeded which lasted until 83 ± 47 ms after stimulus onset, followed by subsequent dSpike failures (Fig. 3b). Sustained spiking led to

very few dSpikes later than 100 ms after stimulus onset, regardless of stimulus strength or location.

We then used a wide-field optogenetic stimulus to test whether stronger depolarization could extend the dSpike time-window. To our surprise, the wide-area stimulus reliably evoked a period-doubling bifurcation: bAPs alternately succeeded and failed to evoke dSpikes ($n$ = 9 cells from 9 animals, Fig. 3c, d). Despite the stronger stimulus, the dSpike window only persisted to ~180 ms after stimulus onset, after which all bAPs failed to evoke dSpikes (Fig. 3e). Even stronger stimuli evoked an epoch of seemingly random interplay of bAPs and dSpikes (Fig. S5), similar to previously reported stochastic backpropagation.[17]

We next sought to determine the biophysical basis of the opening of the dSpike window 18 ± 7 ms after stimulus onset; the closing of the dSpike window 83 ± 47 ms after stimulus onset; and the period-doubling bifurcation upon wide-area stimulation. Motivated by prior studies of dendritic excitability,[24,25] we hypothesized that opening of the dSpike window was driven by inactivation of A-type $K_V$ channels. These transient $K^+$ channels are expressed at a ~6-fold higher level in distal dendrites than in soma.[24] Subthreshold depolarization closes these channels with a voltage-dependent time constant between 6 ms (at -25 mV) and 27 ms (at +55 mV).[24]

To test the involvement of A-type $K_V$ channels, we applied the potassium channel blocker 4-AP (5 mM) and applied optogenetic stimulation at the soma (20 ms duration, 5 Hz, 59 repeats). We observed a significant increase in dSpike probability compared to the baseline (control: 19 ± 8%, 4-AP: 92 ± 9%, mean ± s.e.m., $n$ = 4 cells from 3 animals, $p$ = 0.001, paired t-test; Fig. S6). These results are consistent with previous literature suggesting that A-type $K_V$ channel inactivation opens the dendritic spike window at distal dendrites.[24,26]

We further hypothesized that the closing of the dSpike window was driven by dendritic $Na_V$ channel slow inactivation, leading to a decrease in dendritic excitability after sustained activity.[16] Dendritic $Na_V$ slow inactivation time constants range from 216 ms at 10 Hz spike rate to 58 ms at 50 Hz.[27] To test the involvement of $Na_V$ channels, we applied the $Na_V$ channel blocker TTX at very low concentration (20 nM). Here we stimulated relatively large area to increase the baseline dSpike probability (~100 µm diameter across the soma and proximal dendrites, 20 ms duration, 5 Hz, 59 repeats). This low TTX dose did not affect spiking at the soma, but the mean dSpike probability was significantly decreased (control: 44 ± 15%, TTX: 11 ± 8%, mean ± s.e.m., $n$ = 4 cells from 3 animals, $p$ = 0.008, paired t-test; Fig. S7). In some experiments, a higher concentration of TTX (100 nM) eliminated all dSpikes at distal dendrites, while preserving somatic spiking (Fig.

S8). These data confirm that dSpikes are primarily mediated by $Na^+$ currents and suggest that $Na_V$ inactivation is a plausible trigger to close the dSpike window.

We then simulated a multi-compartment conductance-based model of a CA1 pyramidal neuron, using biophysically realistic ion channels, modified from Ref. [28] (Methods, Fig. S9). To reproduce our data, we augmented the model of the dendritic $Na_V$ channels with a slow inactivation gate; and we adjusted the spatial distributions of dendritic A-type and $Na_V$ channels. After tuning the model, a simulated step-wise optogenetic stimulation at the soma led to a dSpike motif of failure, success, success, failures (Fig. 3f) which closely matched our data (Fig. 3a). Simulated wide-field optogenetic stimulation with the same model parameters evoked a period-doubling bifurcation with alternating dSpike successes and failures, followed by repeated failures (Fig. 3g), matching our observations with wide-field stimulation (Fig. 3c). We conclude that the numerical model accurately captured the dynamics of a CA1 pyramidal dendritic tree.

The simulations reported the contributions of each channel type to the dynamics, confirming that the dSpike window was opened by A-type $K_V$ inactivation and closed by slow $Na_V$ inactivation. Together, these two channels acted as a high-pass filter on the spike rate, allowing a step-wise increase in spike rate at the soma to trigger a transient burst of dSpikes. The simulations also explained the period-doubling: Under simultaneous distal and proximal stimulation, the absolute refractory period of the distal dendrites slightly exceeded the refractory period of the soma. Consequently, after a successful dSpike, the dendrites were still recovering when the next bAP arrived.

Motivated by the parsimonious explanation of the seemingly complex dendritic phenomenology, we developed a coarse-grained two-compartment Izhikevich-type model which also captured the opening and closing of the dSpike window and the period-doubling under simultaneous distal and proximal stimulation (Fig. S10). Such a model may be useful for large-scale simulations of neural dynamics with semi-realistic dendrites.

**Plateau potentials are evoked by collision of synaptic inputs and bAPs**

The experiments with patterned optogenetic stimulation raised a perplexing question: Since bAP and dSpike spatial footprints are each largely insensitive to the stimulus location, then where is the memory trace which determines the specific synapses to potentiate during long-term potentiation? Our voltage imaging experiments ruled out membrane voltage as a primary carrier of the memory trace.

Optogenetic stimulation provides a pure depolarization to the dendrites, without activating any of the ligand-gated channels which are engaged during synaptic transmission. In particular, NMDA receptors show voltage-dependent gating only if first bound to glutamate.[29] To determine how glutamatergic inputs affected dendritic electrophysiology,

we performed additional experiments combining synaptic stimulation, optogenetic stimulation, and dendritic voltage imaging.

We used electric field stimulation (EFS; 0.1 ms, single pulses, 10-40 V) to activate presynaptic axon terminals in the temporoammonic pathway that synapses onto the distal dendrites. We sequentially applied optogenetic stimulation to the soma alone (30 ms), EFS alone, or EFS and optogenetic stimulation. As before, the optogenetic stimulation alone evoked two bAPs followed by a bAP with a dSpike (Fig. 4b). EFS alone evoked a distal depolarization and a single bAP, which often triggered a dSpike. Remarkably, combining optogenetic and electrical stimuli evoked a long-lasting (~120 ms) plateau potential in the dendrites and a burst of spikes on top of a strong subthreshold depolarization at the soma, resembling a complex spike.[30,31] This behavior was qualitatively different from the combined soma + distal dendrite optogenetic stimulation (Fig. 2h), pointing to a critical role of a glutamate-gated channel in the process.

We compared the area under the curve (AUC) for the waveforms at distal dendrites (> 200 µm) induced by optical, electrical, and combined stimulation. The average $AUC_{combined}$ was 3.1 ± 0.7-fold greater than $AUC_{optical}$ + $AUC_{electrical}$ (mean ± s.e.m.) and for more than half of the cells studied (15 of 28 cells from 12 animals), $AUC_{combined}$ was more than twice $AUC_{optical}$ + $AUC_{electrical}$ (Fig. 4d). We characterized in detail the response properties of a subset of cells that showed this > 200% nonlinearity. The nonlinear amplification was greatest when the optical and electrical stimuli overlapped in time (*n* = 8 cells from 7 animals; Fig. 4e and Fig. S11). The decay in amplification was an asymmetric function of the time offset: For 'EFS before bAPs', the decay followed a sigmoidal profile, decaying by half in 87 ms. For 'EFS after bAPs', the decay was better fit by an exponential with a time constant of 35 ms.

We also tested how the number of optogenetically evoked APs affected the nonlinear amplification. Triggering a single bAP by a 10 ms optogenetic stimulus targeted to the soma did not evoke a nonlinear dendritic response, regardless of timing relative to the EFS (*n* = 5 cells from 4 animals; Fig. 4c, e). These results show that multiple bAPs are required to trigger dendritic plateau potentials, likely through dSpikes.

We applied a variety of channel blockers to investigate the molecular mechanisms underlying dendritic plateau potentials. Bath application of blockers for NMDARs (D-AP5, 50 µM; *n* = 6 cells from 5 animals), $Na_V$ channels (TTX, 20 nM; *n* = 4 cells from 3 animals), or voltage-gated $Ca^{2+}$ channels (VGCCs) ($NiCl_2$, 100 µM; *n* = 4 cells from 4 animals) largely eliminated the plateau potential, compared to vehicle control (*n* = 11 cells from 8 animals; Fig. 4f-g). For example, the plateau area was reduced to 42 ± 7% from baseline (mean ± s.e.m.) in the presence of D-AP5 (50 µM) compared to vehicle control (107 ± 5%

of baseline; $p < 0.001$, one-way ANOVA with Bonferroni's *post hoc* test). The drug effects were specific to the plateau: the drug effects on the AUC for EFS or optogenetic stimulation alone were not statistically significant (Fig. S12). These results imply that $Na^+$-dependent dSpikes facilitate VGCC- and NMDAR-dependent dendritic spikes, and these three events cooperatively lead to the plateau (Fig. 4h).

## Discussion

High-resolution voltage imaging and optogenetics revealed the spatial structures of dendritic excitations. We had initially expected to observe dendrite-specific excitations contributing to nonlinear dendritic integration; and to see an influence of optogenetic stimulus location on the bAP propagation, e.g., favoring propagation along the stimulated branch. Under the conditions of our experiments, however, all nonlinear excitations emanated from the soma, and bAP dynamics were highly stereotyped, comprising only two footprints: bAPs alone, and bAPs with broadly distributed dendritic sodium spikes (dSpikes). Information on the spatial structure of the optogenetic inputs was largely absent from the bAPs and the dSpikes; rather dSpikes appeared as a broadcast signal, covering the dendritic tree.

While bAPs and dSpikes carried little spatial information, they had rich temporal encoding. Depolarization of distal dendrites opened a transient window for bAPs to trigger dSpikes, governed by the balance of A-type $K_V$ and $Na_V$ channel availabilities. In a polarized dendrite, A-type channels shunted the voltage, suppressing bAP propagation. One or two bAPs, or direct distal depolarization, could transiently inactivate this shunt, opening a path for subsequent bAPs to engage dendritic $Na_V$ channels and trigger dSpikes. $Na_V$ inactivation then returned the dendrites to a non-excitable state. These biophysical dynamics implemented a spike-rate accelerometer in the dendrites: an accelerating spike rate opened the dSpike window even in the absence of distal inputs, while sustained high-frequency spiking shut it. Our data and the associated model explain the seemingly disparate literature reports on facilitation[15], depression[16], and stochasticity[17] in bAP propagation.

Under concurrent optogenetic stimulation of soma and dendrites, the absolute refractory period of the dendrites was greater than that of the soma, leading to a characteristic period-doubling bifurcation, and then chaotic dynamics in the dendrites even while the somatic spiking remained periodic. The progression from 1:1 conduction, to period-doubling, and ultimately to chaos is a common feature of quasi-one-dimensional excitable chains. Similar dynamics lead to cardiac alternans and arrhythmia,[32] and have been observed in engineered chains of excitable 'spiking HEK' cells which expressed only a sodium and a potassium channel.[33] The stochastic dendritic back-propagation reported previously[17] is more precisely dynamical chaos, where the residue of inactivated $Na_V$

channels from one bAP provides a feedback onto the propagation of the next. It is currently not known whether period-doubling and chaos are relevant to bAP propagation *in vivo*.

The dramatic disparity in electrical responses between distal optogenetic vs. synaptic stimulation showed the key role of NMDA receptors (NMDARs) in dendritic excitability. Simultaneous NMDAR gating by glutamate and voltage-dependent magnesium unblock implemented a pre- and post-synaptic coincidence detector.[34] The presynaptic glutamate signal had high spatial resolution, but comparatively slow temporal resolution (approximately 100 ms); the postsynaptic dSpike had millisecond time resolution, but little spatial information. NMDAR activation was both spatially localized and depended on an accelerating spike rate, thereby tagging synapses likely to have contributed causally to the neuronal output. While dSpikes alone were only 1–2 ms wide, NMDAR-mediated dendritic plateau potentials and associated somatic complex spikes lasted > 100 ms (Fig. 4), likely driving high local calcium influx and thereby local synaptic plasticity. The complex spikes we observed in slices closely resembled the complex spikes which can trigger new place cell formation *in vivo*,[31,35,36] and which have been shown to depend on activation of NMDARs and VGCCs.[37]

The rapid facilitation and then depression of dendritic excitability closely resembles presynaptic facilitation rules.[38] Together these rules imply that pairing of isolated pre- and post-synaptic spikes should be far less efficient at inducing plasticity than is pairing of bursts. Indeed, theta-burst stimulation is the standard approach for eliciting LTP in acute slices.[39] Our model shows how high-frequency bursts of presynaptic stimulation, separated by intervals for recovery of both presynaptic vesicle pools and post-synaptic dendritic $Na_V$ channels, are optimal for triggering dSpikes and plateau potentials. We speculate that the ~8 Hz modulation of dendritic potential by physiological theta rhythms[40] may play a role in resetting dendritic $Na_V$ channels and restoring dendritic excitability.

Our simple biophysical model shows how a distal subthreshold depolarization, timed to coincide with spikes at the soma, can prime the dendrites to produce dSpikes and, if paired with synaptic glutamate, ultimately create plateau potentials. This model provides a biophysical basis for an associative plasticity rule in which inputs from entorhinal cortex on distal dendrites gate plasticity of inputs from CA3, which primarily synapse onto basal and proximal apical dendrites.

Our results suggest that dendritic nonlinearities are primarily relevant to plasticity rules, rather than to rapid integration. Indeed, we propose that distal A-type $K_V$ currents may actively suppress dendrite-initiated dSpikes: the 6-27 ms time-constant for A-type

channels to inactivate[24] was slow enough that distal inputs were guaranteed to trigger a spike at the soma before the dendrites became directly excitable.

Neurons *in vivo* receive inhibitory and neuromodulatory inputs that could modify the simple picture presented here. Branch-specific inhibition, NMDAR activation, or modulation of other ion channels might lead to more branch-to-branch variability in voltage dynamics. However, we recently performed simultaneous voltage imaging in soma and dendrites of Layer 2/3 pyramidal cells *in vivo* and observed highly correlated voltages across the dendritic tree, and a biphasic bAP propagation amplitude similar to our observations here (Fig. 3b).[41] Further study is required to map dendritic integration and back-propagation in CA1 pyramidal cells in live animals.

**Acknowledgments**
We thank A. Preecha and S. Begum for technical assistance, F. P. Brooks for assistance with software, and B. Sabatini for helpful discussions. This work was supported by a Vannevar Bush Faculty Fellowship, a Brain Research Foundation Scientific Innovations Award, the Harvard Brain Science Initiative, and NIH grants R01-NS126043 and R01-MH117042. J.D.W.-C. is a Merck Awardee of the Life Sciences Research Foundation. J. B. G., S. E. P. and L. D. L. are supported by the Howard Hughes Medical Institute.

## Methods

### Genetic constructs

We used Voltron2, an improved chemigenetic voltage indicator[19], and co-expressed it with a blue-shifted channelrhodopsin, CheRiff by a self-cleaving p2a linker. To optimize expression and dendritic membrane trafficking we designed the construct CAG::LR-Voltron2-TS-ER2-p2a-LR-CheRiff-TS-eYFP-ER2 (Addgene: #203228). In this construct, LR is the membrane localization signal from Lucy-Rho[20], TS is the trafficking sequence from $K_{ir}2.1$[21], and ER2 is the endoplasmic reticulum export signal FCYENEV[21]. In some experiments, we used a Cre recombinase-dependent DIO (double-floxed inverse open reading frame) construct, CAG::DIO-LR-Voltron2-TS-ER2-p2a-LR-CheRiff-TS-eYFP-ER2 (Addgene: #203229), and co-expressed it with CAG::Cre (Addgene: #13775; plasmid wt/wt = 30:1 for *in utero* electroporation). Results from both approaches were similar, so the data were pooled.

The genes were cloned into an adeno-associated virus (AAV) backbone with a synthetic CAG promoter using standard Gibson Assembly. Briefly, the vector was linearized by double digestion using restriction enzymes (New England Biolabs) and purified by the GeneJET gel extraction kit (ThermoFisher). DNA fragments were generated by PCR amplification and then fused with the backbones using NEBuilder HiFi DNA assembly kit (New England Biolabs). All plasmids were verified by sequencing (GeneWiz).

**In utero electroporation (IUE)**

All animal procedures adhered to the National Institutes of Health Guide for the care and use of laboratory animals and were approved by the Harvard University Institutional Animal Care and Use Committee (IACUC). The IUE surgery was performed as described previously.[42] Timed-pregnant female CD1 mice (embryonic day 15.5, E15.5; Charles River) were deeply anesthetized and maintained with 2% isoflurane. The animal body temperature was maintained at 37 °C. Uterine horns were carefully exposed and periodically rinsed with warm phosphate-buffered saline (PBS). Plasmid DNA was diluted in PBS (2 µg/µL; 0.05% fast green), and 1 µL of the mixture was injected into the left lateral ventricle of the embryos. Electrical pulses (40 V, 50 ms duration) targeting the hippocampus were delivered five times at 1 Hz using tweezers electroporation electrodes (CUY650P5; Nepa Gene). Injected embryos were returned to the abdominal cavity, and the surgical incision was closed with absorbable PGCL25 sutures (Patterson).

**Slice preparation**

Coronal slices (300 µm) were prepared from CD1 mice of either sex between 2-4 postnatal weeks. Animals were anesthetized with isoflurane and euthanized by decapitation. The brain was then removed and placed in ice-chilled slicing solution containing (in mM): 210 sucrose, 3 KCl, 26 $NaHCO_3$, 1.25 $NaH_2PO_4$, 5 $MgCl_2$, 10 D-glucose, 3 sodium ascorbate, and 0.5 $CaCl_2$ (saturated with 95% $O_2$ and 5% $CO_2$). Acute slices were made using a Vibratome (VT1200S, Leica) while maintained in the slicing solution. Slices were recovered at 34 °C for 10 min in the imaging solution (artificial cerebrospinal fluid, ACSF) containing (in mM): 124 NaCl, 3 KCl, 26 $NaHCO_3$, 1.25 $NaH_2PO_4$, 2 $MgCl_2$, 15 D-glucose, and 2 $CaCl_2$ (saturated with 95% $O_2$ and 5% $CO_2$). Slices were then incubated in ACSF containing $JFX_{608}$-HaloTag ligand[43] (0.5-1 µM) for 30 min at room temperature, and moved to a fresh ACSF for another 30 min to wash out excess dye. Slices were maintained at room temperature until recordings were made.

**Electrophysiology**

Somatic whole-cell recordings were acquired from hippocampal CA1 pyramidal neurons using a custom upright microscope. All experiments were performed at 34 °C, and continuously perfused at 2 mL/min with ACSF. Patch pipettes (2–4 MΩ) were filled with an internal solution containing (in mM): 8 NaCl, 130 $KMeSO_3$, 10 HEPES, 5 KCl, 0.5 EGTA, 4 Mg-ATP, and 0.3 $Na_3$-GTP. The pH was adjusted to 7.3 using KOH and osmolality was adjusted to 285–295 mOsm/L with water. Signals were amplified using a Multiclamp 700B (Molecular Devices), filtered at 10 kHz with the internal Bessel filter, and digitized at 100 kHz using a PCIe-6323 (National Instruments) A/D board. Action potentials (APs) were elicited by a current injection of 2 nA (2 ms duration) in current-clamp mode.

For the experiments in Fig. 4, we applied electric field stimulation (EFS) to the temporoammonic (TA) pathway to evoke synaptic responses. We used a concentric bipolar electrode (CBAPB50, FHC) with stimuli of 10-40 V, 0.1 ms duration. Stimulus intensity was set high enough to obtain plateau potentials when combined with optogenetic stimulation at the soma (30 ms duration), but low enough to not evoke multiple bAPs and plateau potentials by EFS alone. ACSF contained picrotoxin (50 µM) to prevent $GABA_A$ receptor-mediated currents, and $MgCl_2$ concentration was lowered to 1 mM from 2 mM to enhance NMDA receptor-mediated currents.

**Voltage imaging in custom upright microscope**

Voltage imaging experiments were conducted on a previously described home-built epifluorescence microscope.[22] Briefly, blue (488 nm) light was patterned by a digital micromirror device (DMD) and used for targeted channelrhodopsin stimulation. Stimulated regions were confirmed by fluorescence of the eYFP marker in LR-CheRiff-eYFP. Orange (594 nm) illumination was also patterned by a separate DMD and used for structured illumination voltage imaging and *post hoc* HiLo reconstruction of dendritic morphology.[44] Typical laser intensity for 594 nm was 10-20 $mW/mm^2$. Intensity for 488 was up to 1 $mW/mm^2$.

Laser lines from a blue laser (488 nm, 150 mW, Obis LS) and orange laser (594 nm, 100 mW, Cobolt Mambo) were combined by a dichroic (IDEX, FF506-Di03-25x36) and sent through an acousto-optic modulator (TF525-250-6-3-GH18A, Gooch and Housego) for amplitude control. After the modulator, blue and orange lines were split with a dichroic mirror (IDEX, FF506-Di03-25x36), expanded and sent to two independent DMDs for spatial modulation; one for the blue (Lightcrafter DLP3000, Texas Instruments) and the other for the orange (V-7000 VIS, ViALUX). The DMD planes were recombined via a dichroic mirror and re-imaged onto the sample via a tube lens (U-TLU, Olympus) and a 10x water-immersion objective, NA 0.60 (Olympus XLPLN10XSVMP). Fluorescence was collected by the objective and imaged onto a sCMOS camera (Hamamatsu Orca Flash 4.0) with the appropriate emission filter for the orange (Chroma, ET645/75m, bandpass) and blue (Chroma, ET525/50m, bandpass). Light from the excitation and emission was separated by a multi-band dichroic mirror (IDEX, Di01-R405/488/594-25x36, three bandpasses). Voltage-imaging recordings were acquired at a 1 kHz frame rate. Two-photon (2P) imaging and reconstruction was performed using the same microscope adapted to be combined with the 2P illumination. A 25x water-immersion objective, NA 1.05 (Olympus XLPLN25XSVMP2) was used to increase the spatial resolution. Maximum intensity projections of z-stacks were used to form images of the dendritic arbor. The distance for each recording site is a slight underestimate of the true on-path distance from the soma because we ignored changes along the z-axis.

Drugs were prepared as frozen stock solutions (stored at -20 °C). Drugs were: picrotoxin (Abcam), D-(-)-2-Amino-5-phosphonopentanoic acid (D-AP5, Tocris), tetrodotoxin (TTX, Abcam), $NiCl_2$ (Sigma), and 4-Aminopyridine (4-AP, Abcam). $Ni^{2+}$ is considered a non-selective VGCC blocker, but T-type ($Ca_V3.x$) and R-type ($Ca_V2.3$) are sensitive at the used concentration of $Ni^{2+}$ (100 µM; Fig. 4f,g).[45] Drugs were mixed with ACSF and perfused over the slice for at least 15 min prior to measurements. All treatment groups were interleaved with control experiments. Statistical significance was assessed using (two-tailed) paired or unpaired Student's *t*-tests or one-way ANOVA with Bonferroni's *post hoc* test as appropriate; the level of significance is denoted on the figures as follows: $*p < 0.05$, $**p < 0.01$ and $***p < 0.001$. The experiments were not randomized, and the investigators were not blinded to the experimental condition. Sample size was based on reports in related literature and was not predetermined by calculation.

## Image analysis

All analysis was performed in MATLAB, as described below.

### *Extracting fluorescence from movies*

Fluorescence values were extracted from raw movies in one of two ways. One approach used the maximum-likelihood pixel-weighting algorithm described previously.[18] Briefly, the fluorescence at each pixel was correlated with the whole-field average fluorescence. Pixels that showed stronger correlation to the mean were preferentially weighted. This algorithm automatically found the pixels carrying the most information, and de-emphasized background pixels. Alternatively, a user defined a region comprising the soma and dendrites and calculated fluorescence from the unweighted mean of pixel values within this region. When necessary, photobleaching was corrected by dividing the frames by a regression fit to the mean fluorescence.

### *Spike-triggered average (STA) movies*

A simple threshold-and-maximum procedure was applied for spike detection. Fluorescence traces were first high-pass-filtered and initial threshold was set at three times the noise level. This threshold was then manually adjusted. Neighboring frames (typically 12 frames) were segmented, aligned to the peak, and averaged. We often used stimulus-triggered averages, where the traces were aligned based on the timing of optogenetic stimulus onset.

When necessary, we applied spatial and temporal filters to further decrease the noise in the movies. The spatial filter consisted of convolution with a Gaussian kernel, typically with an s.d. of 5 pixels. The temporal filter was based upon principal-components analysis (PCA) of the set of single-pixel time traces. The time trace at each pixel was expressed in the basis of PCA eigenvectors. Typically, the first five eigenvectors were sufficient to

account for > 99% of the pixel-to-pixel variability in AP waveforms, and thus the PCA eigendecomposition was truncated after five terms. The remaining eigenvectors typically represented uncorrelated shot noise. To verify that the spatial and PCA filtering did not distort the underlying AP waveforms, we compared mean AP waveforms in subcellular compartments before and after the smoothing steps. We observed no systematic deviations in the AP waveforms in the soma or dendrites.

### *Sub-Nyquist Action Potential Timing (SNAPT)*

Spike propagation delay was calculated using the SNAPT subframe interpolation algorithm as described previously.[18] In brief, spike-triggered average (STA) movies were used as a template and fit with a quadratic spline interpolation. The time of spike threshold crossing was calculated for each pixel to create a map of the spike delay. The fits were then converted into movies. Spike timing at each pixel was represented by a brief flash, which followed a Gaussian time course with duration equal to the cell-average time resolution, $\sigma$.

To enhance the spatial resolution of the high temporal resolution movies, we mapped the timing data onto a static 2P structural image. The fluorescence was obtained either by eYFP (from the LR-CheRiff-eYFP fusion) at 920 nm or $JFX_{608}$ HaloTag ligand at 820 nm using a femtosecond tunable pulsed 2P laser (Chameleon Vision II, Coherent). Sometimes we made a structural image using 1P HiLo reconstruction tool (Fig. 3a, c).[44] The pixel matrix of the subframe interpolated movie was expanded to match the dimensions of the high-resolution image, and the amplitude at each pixel was then set equal to the mean brightness at that pixel. For assembly of the color movies, the timing signal was assigned to a color map that was overlaid on a grayscale image of mean fluorescence. The optically stimulated region of the cell was highlighted in blue.

### *Normalization to reference signal ($\Delta F/F_{ref}$)*

Basal fluorescence, $F_0$, was not homogeneous across soma and dendrites. This might be due to a variability in intracellular protein, membrane trafficking, and/or $JFX_{608}$ HaloTag ligand staining. Therefore, instead of estimating signal amplitude via $\Delta F/F_0$, we normalized the signal, $\Delta F$, by the amplitude of the change in fluorescence during the passive return to baseline after a stimulus (i.e., $\Delta F/F_{ref}$; Fig. 1d). $\Delta F/F_{ref}$ was used for all spike amplitude heatmaps and kymographs unless stated otherwise.

### *Kymograph*

We manually drew a line along the apical dendrite and then determined the mean fluorescence time-course in equal-length segments along the line. Typical segment size was 10 pixels (6.5 µm with 10x objective). The fluorescence waveforms were assembled into a kymograph matrix showing signal amplitude as a function of linear position and

time. Example waveforms were calculated by averaging responses from 5 segments (~33 μm contour length) and plotted on top of the kymographs.

### *Counting bAPs and dSpikes*

All spikes above a user-defined threshold at the soma were counted as back-propagating action potentials (bAPs). The timing of each bAP was estimated relative to the optogenetic stimulation onset. Dendritic spikes (dSpikes) were detected using the same procedure of high-pass-filter and simple threshold-and-maximum in a user-defined region (typically > 300 μm from soma). Initial threshold was set at two times the subthreshold depolarization. This threshold was then manually adjusted. We defined dSpikes as a large and narrow discharge (typically < 5 ms in full width at half maximum). DSpike successes and failures were clearly distinguished in the fluorescence traces (e.g., Fig. 2d).

### *Period doubling bifurcation*

We typically observed period doubling during wide-field optogenetic stimulation (Fig. 3c-e). However, overly strong stimulation frequently led to the failure of all spikes, likely due to incomplete recovery of $Na_V$ channels. Prior to experiments, we determined an optimal stimulation intensity to clearly observe the bifurcation. The frequency of bAPs was estimated by measuring the time interval between bAP peaks, while the amplitude was normalized to average of the final 5 bAPs in a stimulus epoch (Fig. 3e).

### *Normalization of plateau potential area*

The cumulative area under the curve (AUC) was determined by integrating fluorescence changes, ΔF, with respect to time (Fig. S11). In Fig. 4d, the normalized area (% sum) was calculated as AUC for combined stimulation ($AUC_{combined}$), divided by the sum of the AUC for optogenetic stimulation alone ($AUC_{optical}$) and the AUC for EFS alone ($AUC_{electrical}$). In Fig. 4e, the normalized area (% peak) was calculated by mapping the AUC for combined stimulus for each cell vs. ΔTime to the range [0, 1] (Fig. S11b-c). In Fig. 4g, the normalized area (% baseline) was determined as the ratio of AUC to baseline AUC prior to any vehicle or drug treatment. To compare the effects, drugs were applied for at least 15 min in the bath before measurement.

## Biophysical modeling

### *Simulating a CA1 pyramidal cell in NEURON*

Morphologically realistic simulations were carried out on an AMD64-Windows computer using NEURON[46] through its Python interface (Python 3.11, NEURON 8.2) and exported into MATLAB to analyze and compare with experimental data. We adapted an existing CA1 pyramidal cell model (ModelDB accession number: 116084)[28] by introducing slow

$Na_V$ inactivation, fine-tuning ion channel parameters and spatial distributions, and introducing channelrhodopsin.

Model specifications and simulation code are available as Supplementary Files.

***Model properties***

Our modified model uses the same morphology and channel types as ref. 27: $Na_V$ channels, A-type $K_V$ channels and delayed rectifier $K_{DR}$ channels. We modified the published model by adding a slow inactivation gate to the $Na_V$ channels, varying the distributions of $Na_V$ channels and A-type $K_V$ channels, adding a gradient in the maximal $Na_V$ inactivation from soma to the distal dendrites, and adding a model of a channelrhodopsin in the somatic and dendritic compartments. The A-type $K_V$ channels were separated into two subtypes, with one subtype located in the proximal dendrites (less than 100 μm from the soma) and another in the distal dendrites. The subtypes differed slightly in the kinetics and voltage dependence of the activation variable, to reproduce measured channel properties and distributions in CA1 pyramidal dendrites.[24] Optogenetic stimulation was implemented using distributed time-dependent conductances. Channel densities and other parameters are summarized in Table 1 and Fig. S9.

**Table 1: Ion channel densities in a model CA1 pyramidal cell.** Channel models were adapted from Ref. [28].

| Channel Properties | Value | Location / Condition |
|---|---|---|
| $Na_V$ density ($\bar{g}_{NaV}$) | 30 mS/cm$^2$ | Axon (nodal compartments) |
| $Na_V$ density ($\bar{g}_{NaV}$) | 0.051 - 0.048 mS/cm$^2$ | Ramp decrease from soma to distal dendrites. Axon (outside of nodes) |
| Slow $Na_V$ inactivation | 0% | Basal dendrites and proximal apical dendrites until 340 μm |
| Slow $Na_V$ inactivation | 0% up to 70% | Ramp increase from 340 μm to 700 μm in apical dendrites |
| A-type $K_V$ channels ($\bar{g}_{KA}$) | 0.048 - 0.33 mS/cm$^2$ | Ramp increase with distance from soma to apical dendrites, plateauing after 400 μm |
| A-type $K_V$ channels ($\bar{g}_{KA}$) | 0.0096 mS/cm$^2$ | Axon (nodal and internodal compartments) |
| Delayed rectifier $K_{DR}$ channels ($\bar{g}_{KDR}$) | 0.04 mS/cm$^2$ | Homogeneous across all compartments |
| Membrane capacitance | 0.75 μF/cm$^2$ | All compartments except axon (internodal) |

| Channel Properties | Value | Location / Condition |
|---|---|---|
| Membrane capacitance | 0.04 μF/cm$^2$ | Axon (internodal compartments, myelinated) |

In the apical dendritic arbor, A-type $K_V$-channel densities increased linearly with distance from $\bar{g}_{KA}$ = 0.048 mS/cm$^2$ at the soma to $\bar{g}_{KA}$ = 0.33 mS/cm$^2$ at 400 μm, consistent with patch clamp measurements.[24] Thereafter the density was kept constant.

The $Na_V$ channels were distributed throughout the soma, axon, and dendrites, with a much higher density in the axonal nodes of Ranvier ($\bar{g}_{NaV}$ = 30 mS/cm$^2$) than in the dendrites and other compartments ($\bar{g}_{NaV}$ ≈ 0.05 mS/cm$^2$). In our model, these channels exhibited fast inactivation over the course of a bAP, and also distance-dependent slow inactivation, which contributed to dSpike failures after several successful dSpikes. The apical channel density linearly decreased from $\bar{g}_{NaV}$ = 0.051 mS/cm$^2$ at the soma to $\bar{g}_{NaV}$ = 0.048 mS/cm$^2$ at 600 μm, after which it was constant. No slow $Na_V$ inactivation was present in the basal dendrites and proximal apical dendrites until 340 μm. Between 340 μm and 700 μm, the maximum permitted inactivation increased linearly up to 70% (i.e., at most 70% of the $Na_V$ conductance could be inactivated in the distal dendrites).

$K_{DR}$ channels were homogeneously distributed across all compartments with a density of $\bar{g}_{KDR}$ = 0.04 mS/cm$^2$.

While the channel densities required some fine-tuning, a variety of $Na_V$ and A-type $K_V$ profiles reproduced the experimental results. The $Na_V$ gradient could be increasing or decreasing, but always needed to be accompanied by a steep increase of A-type $K_V$ conductance towards the distal dendrites.

**Table 2: Simulated spiking patterns evoked by different patterns of channelrhodopsin stimulation.** The simulated ChR conductance was turned on for 185 ms, and the voltage dynamics in the soma and distal dendrites were calculated.

| | Channelrhodopsin conductance (gChR) | | | |
|---|---|---|---|---|
| **dSpike pattern** | **Somatic compartment** | **Basal and < 200 μm apical** | **200-700 μm apical** | **Apical >700 μm** |
| F F F F F F … | 0.45 mS/cm$^2$ | 0 | 0 | 0 |
| F S F F F F … | 0.54 mS/cm$^2$ | 0 | 0 | 0 |
| F S F F F F … | 0.90 mS/cm$^2$ | 0 | 0 | 0 |
| F S S S F F … | 1.50 mS/cm$^2$ | 0 | 0 | 0 |
| F S F S F S … | 2.40 mS/cm$^2$ | 0.60 mS/cm$^2$ | 0.30 mS/cm$^2$ | 0.15 mS/cm$^2$ |
| F S F S F S… | 3.00 mS/cm$^2$ | 0 | 0 | 0 |

### *Channelrhodopsin*

Table 2 shows the results of various simulated optogenetic stimulation regimes. Stimulation at the soma (185 ms duration) successfully recreated the bAP propagation profiles seen in the experiment (Fig. 3). Further in agreement with experimental observations, more intense somatic stimulation created multiple successful bAPs. No successful dSpikes were observed for $g_{ChR} < 0.45$ mS/cm$^2$ at the soma. Channelrhodopsin conductances of $g_{ChR} = 0.54$ mS/cm$^2$, 0.90 mS/cm$^2$, and 1.50 mS/cm$^2$ at the soma resulted in one, two (Fig. 3f), or three successful dSpikes, respectively. A strong somatic simulation with $g_{ChR} = 3.00$ mS/cm$^2$ or additional widefield stimulation (soma = 2.40 mS/cm$^2$; basal and < 200 μm apical = 0.60 mS/cm$^2$; apical between 200-700 μm = 0.30 mS/cm$^2$; and apical > 700 μm = 0.15 mS/cm$^2$) reproduced the observed period-doubling bifurcation. Stimulation conductances in the distal regions were kept low to avoid driving the dendrites into depolarization block (0.15 mS/cm$^2$ compared to >2 mS/cm$^2$ in the somatic compartment).

Although the model lacks voltage-gated calcium channels (VGCCs) and NMDARs, it still reproduced the main phenomenology of optogenetically evoked bAPs and dSpikes. This observation supports the view that bAP gating is primarily mediated by dendritic A-type $K_V$ channels and $Na_V$ channels. The VGCCs appeared to be primarily involved in amplifying plateau potentials, a phenomenon we did not simulate.

### Coupled two-compartment Izhikevich model

As a complement to the morphologically and physiologically detailed CA1 model, we introduced a two-stage resistively coupled Izhikevich model (Fig. S10). Despite its simplicity, this model broadly reproduced the bAP filtering characteristics of the CA1 dendrites. The classical Izhikevich model is a computationally efficient spiking neuron model consisting of a voltage variable *v* and a slow adaptation variable *u*, and is capable of reproducing a wide variety of neuronal behaviors observed in mammalian brains.[47] These characteristics made it an attractive starting point for a simplified CA1 model.

In our adaptation of the Izhikevich model, the soma was tuned to exhibit regular spiking without adaptation. The soma was resistively coupled to the dendrite compartment that featured an adjusting spiking threshold. Optogenetic-like stimulation was implemented as variable conductances with 0 mV reversal potential at the soma or dendrites. When the model was driven by optogenetic stimulation at the soma only, it replicated the behavior seen in Fig. 3a. A single spike from the soma did not depolarize the dendrites enough to trigger a spike, but a spike train from the soma was able to evoke dendritic spikes. The spike-threshold adaptation in the dendrites mimicked the effect of $Na_V$ inactivation, causing the dendrites to lose excitability after several successful spikes. The distal dendrites thereby acted as a high-pass filter or accelerometer, selectively responding to a small number of somatic spikes following a step increase in somatic firing rate.

Simultaneous stimulation of soma and dendrites recreated the experimentally observed period-doubling bifurcation shown in Fig. 3b.

Model specifications and simulation code are available as Supplementary Files.

## References


1. Turner, R., Meyers, D., Richardson, T. & Barker, J. The site for initiation of action potential discharge over the somatodendritic axis of rat hippocampal CA1 pyramidal neurons. *J. Neurosci.* **11**, 2270–2280 (1991).
2. Stuart, G. J. & Sakmann, B. Active propagation of somatic action potentials into neocortical pyramidal cell dendrites. *Nature* **367**, 69–72 (1994).
3. Markram, H., Lübke, J., Frotscher, M. & Sakmann, B. Regulation of synaptic efficacy by coincidence of postsynaptic APs and EPSPs. *Science* **275**, 213–215 (1997).
4. Golding, N. L. & Spruston, N. Dendritic Sodium Spikes Are Variable Triggers of Axonal Action Potentials in Hippocampal CA1 Pyramidal Neurons. *Neuron* **21**, 1189–1200 (1998).
5. Magee, J. C. & Johnston, D. Characterization of single voltage-gated Na+ and Ca2+ channels in apical dendrites of rat CA1 pyramidal neurons. *J. Physiol.* **487**, 67–90 (1995).
6. Larkum, M. E., Zhu, J. J. & Sakmann, B. A new cellular mechanism for coupling inputs arriving at different cortical layers. *Nature* **398**, 338–341 (1999).
7. Golding, N. L., Jung, H., Mickus, T. & Spruston, N. Dendritic Calcium Spike Initiation and Repolarization Are Controlled by Distinct Potassium Channel Subtypes in CA1 Pyramidal Neurons. *J. Neurosci.* **19**, 8789–8798 (1999).
8. Takahashi, H. & Magee, J. C. Pathway interactions and synaptic plasticity in the dendritic tuft regions of CA1 pyramidal neurons. *Neuron* **62**, 102–111 (2009).
9. Brandalise, F., Carta, S., Helmchen, F., Lisman, J. & Gerber, U. Dendritic NMDA spikes are necessary for timing-dependent associative LTP in CA3 pyramidal cells. *Nat. Commun.* **7**, 13480 (2016).
10. Schiller, J., Major, G., Koester, H. J. & Schiller, Y. NMDA spikes in basal dendrites of cortical pyramidal neurons. *Nature* **404**, 285–289 (2000).
11. Johnston, D., Magee, J. C., Colbert, C. M. & Cristie, B. R. Active properties of neuronal dendrites. *Annu. Rev. Neurosci.* **19**, 165–186 (1996).
12. Hausser, M., Spruston, N. & Stuart, G. J. Diversity and dynamics of dendritic signaling. *Science* **290**, 739–744 (2000).
13. Spruston, N. Pyramidal neurons: dendritic structure and synaptic integration. *Nat. Rev. Neurosci.* **9**, 206–221 (2008).
14. Major, G., Larkum, M. E. & Schiller, J. Active Properties of Neocortical Pyramidal Neuron Dendrites. *Annu. Rev. Neurosci.* **36**, 1–24 (2013).
15. Larkum, M. E., Kaiser, K. M. M. & Sakmann, B. Calcium electrogenesis in distal apical dendrites of layer 5 pyramidal cells at a critical frequency of back-propagating action potentials. *Proc. Natl. Acad. Sci.* **96**, 14600–14604 (1999).
16. Spruston, N., Schiller, Y., Stuart, G. & Sakmann, B. Activity-Dependent Action Potential Invasion and Calcium Influx into Hippocampal CA1 Dendrites. *Science* **268**, 297–300 (1995).
17. Short, S. M. *et al.* The stochastic nature of action potential backpropagation in apical tuft dendrites. *J. Neurophysiol.* **118**, 1394–1414 (2017).

18. Hochbaum, D. R. *et al.* All-optical electrophysiology in mammalian neurons using engineered microbial rhodopsins. *Nat. Methods* **11**, 825–833 (2014).
19. Abdelfattah, A. S. *et al.* Sensitivity optimization of a rhodopsin-based fluorescent voltage indicator. *Neuron* (2023) doi:10.1016/j.neuron.2023.03.009.
20. Shepard, B. D., Natarajan, N., Protzko, R. J., Acres, O. W. & Pluznick, J. L. A cleavable N-terminal signal peptide promotes widespread olfactory receptor surface expression in HEK293T cells. *PloS One* **8**, e68758 (2013).
21. Gradinaru, V. *et al.* Molecular and Cellular Approaches for Diversifying and Extending Optogenetics. *Cell* **141**, 154–165 (2010).
22. Adam, Y. *et al.* Voltage imaging and optogenetics reveal behaviour-dependent changes in hippocampal dynamics. *Nature* **569**, 413 (2019).
23. Larkum, M. E., Waters, J., Sakmann, B. & Helmchen, F. Dendritic Spikes in Apical Dendrites of Neocortical Layer 2/3 Pyramidal Neurons. *J. Neurosci.* **27**, 8999-9008-8999–9008 (2007).
24. Hoffman, D. A., Magee, J. C., Colbert, C. M. & Johnston, D. K+ channel regulation of signal propagation in dendrites of hippocampal pyramidal neurons. *Nature* **387**, 869-875-869–875 (1997).
25. Magee, J. C. & Johnston, D. A Synaptically Controlled, Associative Signal for Hebbian Plasticity in Hippocampal Neurons. *Science* **275**, 209–213 (1997).
26. Chen, X. *et al.* Deletion of Kv4.2 Gene Eliminates Dendritic A-Type K+ Current and Enhances Induction of Long-Term Potentiation in Hippocampal CA1 Pyramidal Neurons. **26**, 12143–12151 (2006).
27. Mickus, T., Jung, H. & Spruston, N. Properties of Slow, Cumulative Sodium Channel Inactivation in Rat Hippocampal CA1 Pyramidal Neurons. *Biophys. J.* **76**, 846–860 (1999).
28. Jarsky, T., Roxin, A., Kath, W. L. & Spruston, N. Conditional dendritic spike propagation following distal synaptic activation of hippocampal CA1 pyramidal neurons. *Nat. Neurosci.* **8**, 1667–1676 (2005).
29. Kampa, B. M., Clements, J., Jonas, P. & Stuart, G. J. Kinetics of Mg2+ unblock of NMDA receptors: implications for spike-timing dependent synaptic plasticity. *J. Physiol.* **556**, 337–345 (2004).
30. Kamondi, A., Acsády, L. & Buzsáki, G. Dendritic Spikes Are Enhanced by Cooperative Network Activity in the Intact Hippocampus. *J. Neurosci.* **18**, 3919–3928 (1998).
31. Bittner, K. C., Milstein, A. D., Grienberger, C., Romani, S. & Magee, J. C. Behavioral time scale synaptic plasticity underlies CA1 place fields. *Science* **357**, 1033–1036 (2017).
32. Guevara, M. R., Glass, L. & Shrier, A. Phase Locking, Period-Doubling Bifurcations, and Irregular Dynamics in Periodically Stimulated Cardiac Cells. *Science* **214**, 1350–1353 (1981).
33. McNamara, H. M. *et al.* Geometry-dependent arrhythmias in electrically excitable tissues. *Cell Syst.* **7**, 359-370. e6 (2018).
34. Bliss, T. V. P. & Collingridge, G. L. A synaptic model of memory: long-term potentiation in the hippocampus. *Nature* **361**, 31–39 (1993).
35. Fan, L. Z. *et al.* All-optical physiology resolves a synaptic basis for behavioral timescale plasticity. *Cell* **186**, 543-559.e19 (2023).
36. Rolotti, S. V. *et al.* Local feedback inhibition tightly controls rapid formation of hippocampal place fields. *Neuron* **110**, 783-794.e6 (2022).
37. Grienberger, C., Chen, X. & Konnerth, A. NMDA Receptor-Dependent Multidendrite Ca2+ Spikes Required for Hippocampal Burst Firing In Vivo. *Neuron* **81**, 1274–1281 (2014).

38. Jackman, S. L., Beneduce, B. M., Drew, I. R. & Regehr, W. G. Achieving High-Frequency Optical Control of Synaptic Transmission. *J. Neurosci.* **34**, 7704–7714 (2014).
39. Larson, J., Wong, D. & Lynch, G. Patterned stimulation at the theta frequency is optimal for the induction of hippocampal long-term potentiation. *Brain Res.* **368**, 347–350 (1986).
40. Buzsaki, G. Theta oscillations in the hippocampus. *Neuron* **33**, 325–340 (2002).
41. Wong-Campos, J. D. *et al.* Voltage dynamics of dendritic integration and back-propagation in vivo. (2023) doi:10.1101/2023.05.25.542363.
42. Landau, A. T. *et al.* Dendritic branch structure compartmentalizes voltage-dependent calcium influx in cortical layer 2/3 pyramidal cells. *eLife* **11**, e76993 (2022).
43. Lin, D. *et al.* Time-tagged ticker tapes for intracellular recordings. *Nat. Biotechnol.* **41**, 631–639 (2023).
44. Lim, D., Chu, K. K. & Mertz, J. Wide-field fluorescence sectioning with hybrid speckle and uniform-illumination microscopy. *Opt. Lett.* **33**, 1819 (2008).
45. Avery, R. B. & Johnston, D. Multiple Channel Types Contribute to the Low-Voltage-Activated Calcium Current in Hippocampal CA3 Pyramidal Neurons. *J. Neurosci.* **16**, 5567–5582 (1996).
46. Hines, M. L. & Carnevale, N. T. The NEURON Simulation Environment. *Neural Comput.* **9**, 1179–1209 (1997).
47. Izhikevich, E. M. Simple model of spiking neurons. *IEEE Trans. Neural Netw.* **14**, 1569–1572 (2003).

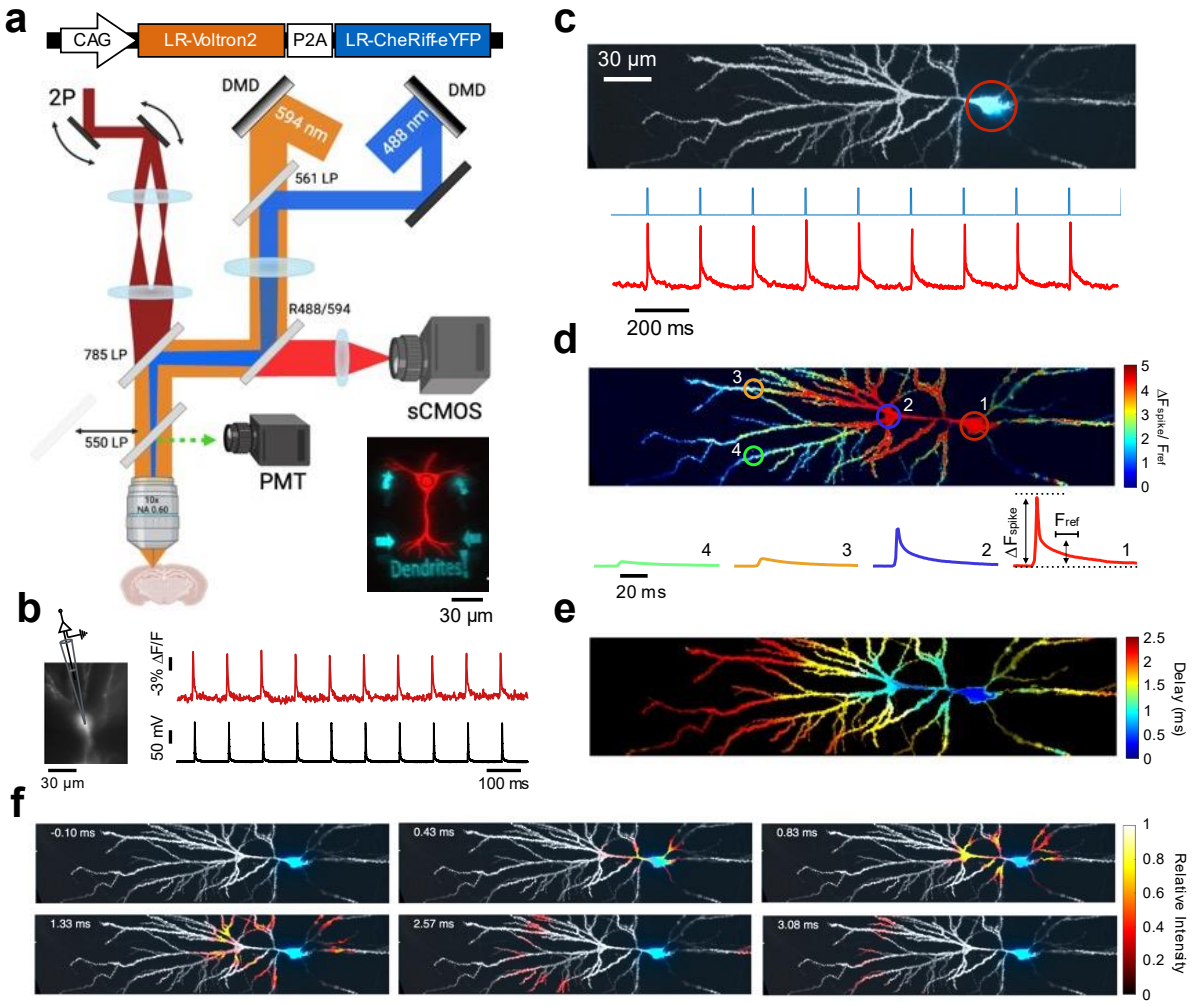


**Fig. 1 | Mapping spike back-propagation with all-optical electrophysiology. a,** Top: genetic construct for co-expression of LR-Voltron2 and LR-CheRiff-eYFP. Bottom: optical system combining two-photon (2P) static structural imaging (dark red), micromirror-patterned dynamic voltage imaging (orange), and optogenetic stimulation (blue). DMD, digital micromirror device. Inset: micromirror-patterned red and blue illumination on a test slide. **b,** Concurrent voltage imaging and whole-cell patch clamp recording at the soma. Sample rates: 1 kHz and 100 kHz, respectively. Spikes evoked by current injection using a patch electrode (2 nA for 2 ms at 10 Hz). **c,** Top: 2P structural image of a CA1 neuron (gray), overlayed with optogenetic stimulus region (blue; 10 ms duration at 5 Hz). Bottom: blue illumination sequence with voltage-dependent fluorescence at the soma (red). **d,** Top: spike amplitude map from spike-triggered average of 59 spikes. Bottom: voltage traces in the correspondingly numbered circled regions. $\Delta F_{spike}$, peak spike amplitude. $F_{ref}$, mean amplitude during the reference time (from t = 10-20 ms after spike, Methods). **e,** Spike delay map. **f,** Sub-frame interpolation showing details of spike back-propagation (see also Movie 1).

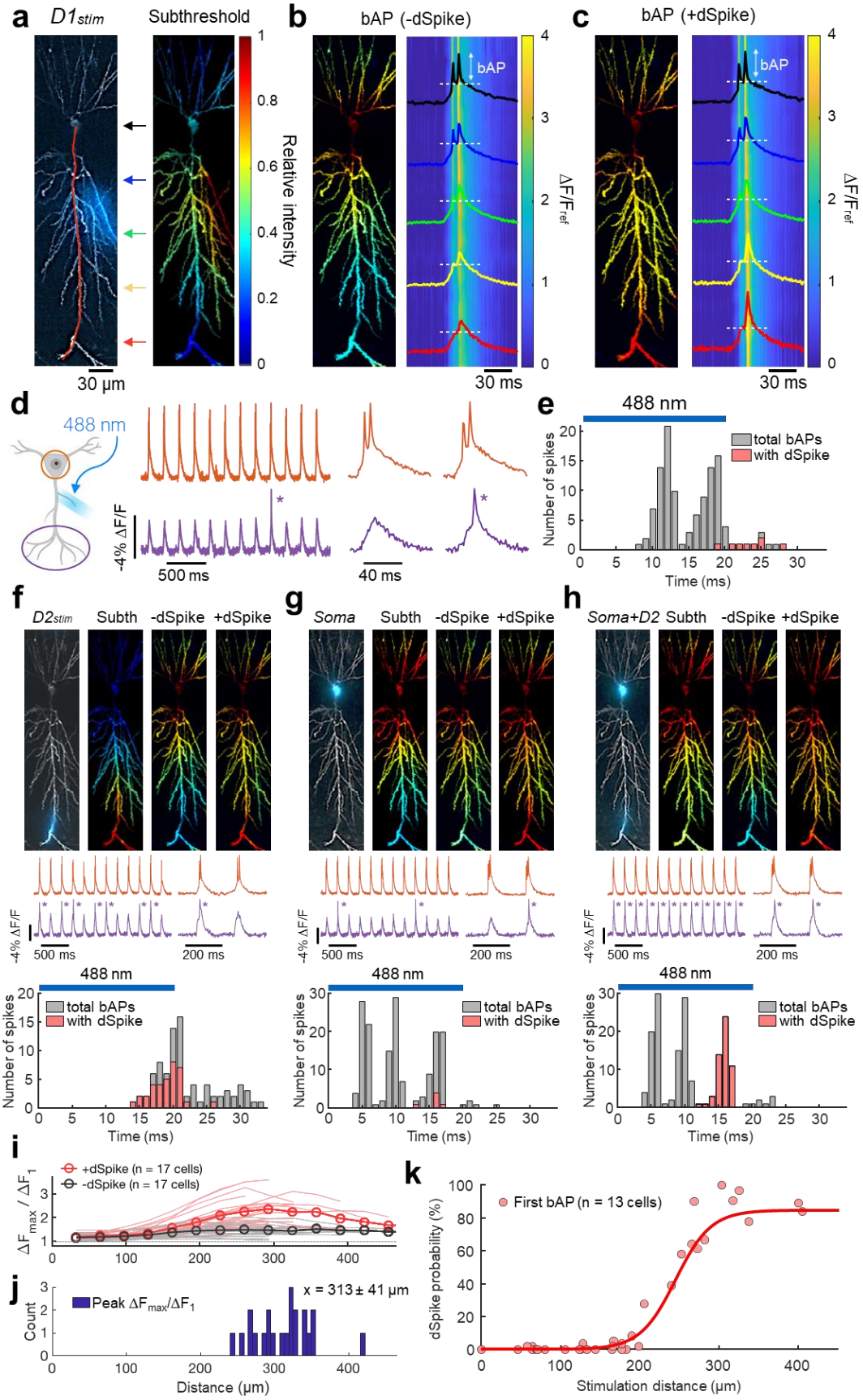
a
D1stim
Subthreshold
Relative intensity
30 µm
b
bAP (-dSpike)
bAP
ΔF/Fref
30 ms
c
bAP (+dSpike)
bAP
ΔF/Fref
30 ms
d
488 nm
-4% ΔF/F
500 ms
40 ms
e
488 nm
total bAPs
with dSpike
Number of spikes
Time (ms)
f
D2stim
Subth
-dSpike
+dSpike
-4% ΔF/F
500 ms
200 ms
488 nm
total bAPs
with dSpike
Number of spikes
Time (ms)
g
Soma
Subth
-dSpike
+dSpike
-4% ΔF/F
500 ms
200 ms
488 nm
total bAPs
with dSpike
Number of spikes
Time (ms)
h
Soma+D2
Subth
-dSpike
+dSpike
-4% ΔF/F
500 ms
200 ms
488 nm
total bAPs
with dSpike
Number of spikes
Time (ms)
i
+dSpike (n = 17 cells)
-dSpike (n = 17 cells)
ΔFmax / ΔF1
j
Peak ΔFmax/ΔF1
x = 313 ± 41 µm
Count
Distance (µm)
k
First bAP (n = 13 cells)
dSpike probability (%)
Stimulation distance (µm)

**Fig. 2 | Spatial and temporal maps of dendritic spikes (dSpikes). a,** Stimulation at a proximal dendritic branch (*$D1_{stim}$*). Left: 2P structural image (gray) combined with the optogenetic stimulus region (blue; 20 ms duration at 5 Hz). Right: normalized amplitude ($\Delta F/F_{ref}$) map for subthreshold depolarization (stimulus-triggered average from 54 trials). Amplitude heatmaps for following panels share the same color scale. **b,** Normalized amplitude ($\Delta F/F_{ref}$) map for back-propagating action potentials (bAPs) without dSpikes (-dSpikes; spike-triggered average from 56 spikes). Right: kymograph for a single-trial example of bAP without dSpike along the red line in (**a**). Sample traces taken from the regions indicated by colored arrows. **c,** Corresponding plots for bAPs with dSpikes (+dSpikes). Normalized amplitude map, spike-triggered average from 8 spikes. **d,** Example traces at the soma (orange) and a distal dendrite (> 300 µm; purple) showing trials without and with a dSpike (*). **e,** Counting all bAPs (gray), and bAPs with dSpikes from the same cell (red), as a function of time after optogenetic stimulus onset. Blue bar shows the stimulus timing. **f-h,** Corresponding plots for stimuli at a distal dendrite (**f**, *$D2_{stim}$*; 54 trials, 19 -dSpikes, and 37 +dSpikes), soma (**g**, *Soma*; 54 trials, 161 -dSpikes, and 6 +dSpikes), and both soma and distal dendrite simultaneously (**h,** *Soma+D2*; 54 trials, 116 -dSpikes, and 54 +dSpikes). **i,** Amplitude ratio of the later bAP compared to the first bAP ($\Delta F_{max}/\Delta F_1$). Data sorted by the presence (+dSpike) vs. absence (-dSpike) of dSpike. Soma or proximal dendritic branch (< 200 µm) was stimulated (*n* = 22 branches, 17 cells, 15 animals). Mean (open circles), individual stimuli (thin lines). **j,** Distance from soma to the area showing peak $\Delta F_{max}/\Delta F_1$ (x = mean ± s.d.), where $\Delta F_1$ is the amplitude of the first spike after stimulus onset and $\Delta F_{max}$ is the amplitude of a subsequent dSpike. **k,** Probability for the first bAP after stimulus onset to trigger a dSpike, as a function of stimulus distance from soma (*n* = 35 dendrites, 13 cells, 11 animals). Red line, sigmoidal fit.

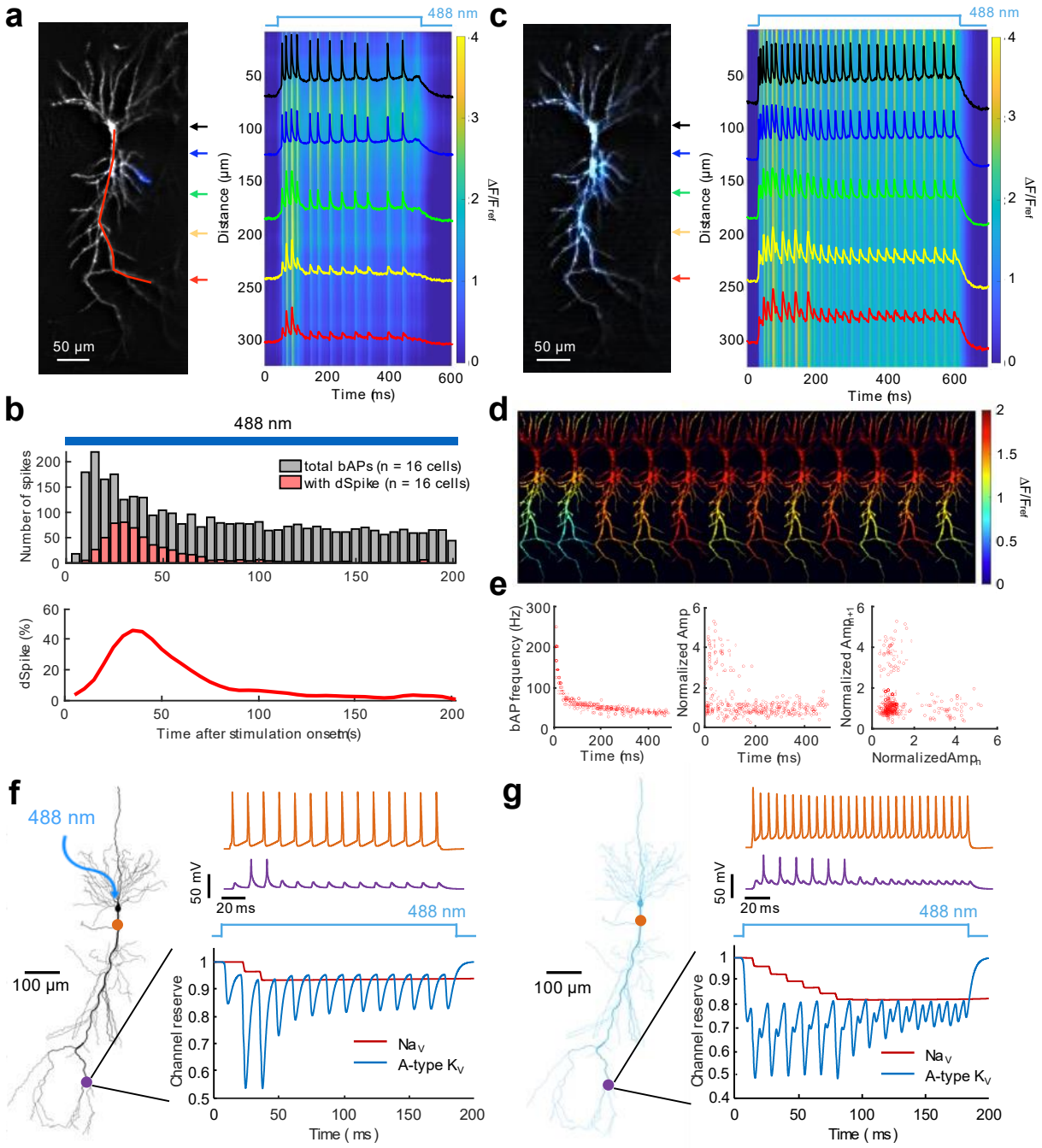


**Fig. 3 | Depolarization opens a window for dSpikes in distal dendrites. a,** Structural image with optogenetic stimulus targeted to a proximal dendrite (blue). Kymograph along the red line. Example traces taken from the regions indicated by colored arrows. **b,** Number of bAPs (grey) and bAPs with dSpikes (red), as a function of time after stimulus onset (*n* = 43 dendrite stimulus locations, 16 cells, and 13 animals). Bottom: Percent of dSpikes among all bAPs. **c,** Equivalent experiment using wide-field illumination which covered the soma and apical trunk (blue). **d,** Amplitude maps of the first 12 bAPs showing

two bAP failures, followed by alternating dSpikes and bAP failsures. **e,** Plots showing period-doubling bifurcations (*n* = 9 cells from 9 animals). Left: bAP frequency as a function of time after stimulation onset. Middle: Normalized bAP amplitude relative to average of the final 5 bAPs. Right: Relationship between amplitudes of successive bAPs, $bAP_{n+1}$ vs. $bAP_n$ showing an alternating motif. **f-g,** Simulations showing spiking at the soma (orange) and distal dendrites (purple) and the dynamics of A-type $K_V$ channels (blue) and $Na_V$ channels (red). **f,** Soma-targeted stimulation opens a transient window for dSpike excitation. **g,** Wide-field stimulation evokes transient period-doubling bifurcation. $Na_V$ channel reserve defined by the slow inactivation gate (fast inactivation and recovery not shown). A-type $K_V$ channel reserve defined by the inactivation variable *l*.

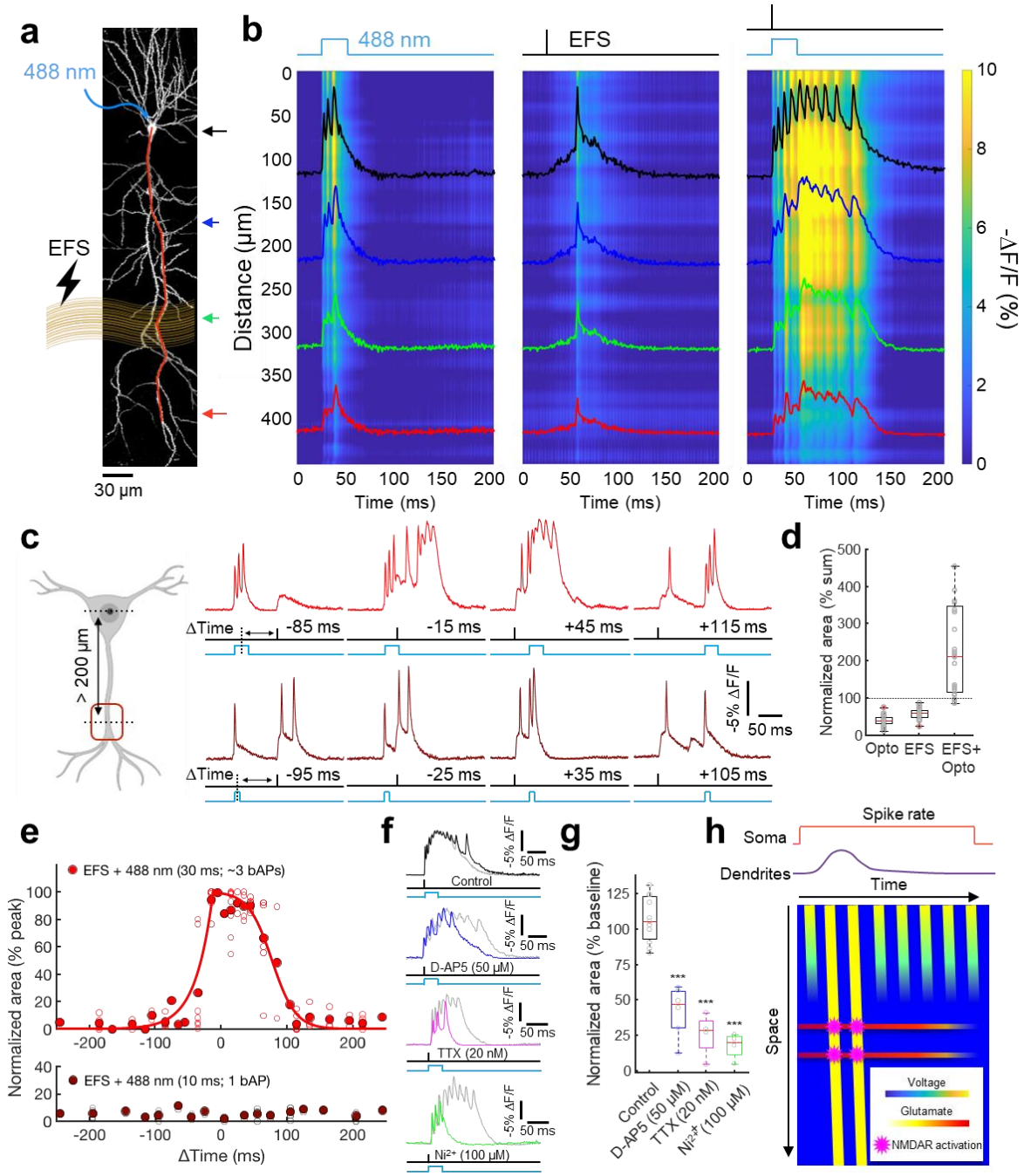


**Fig. 4 | Collision of synaptic inputs and dSpikes triggers plateau potentials. a,** Structural image (gray) showing optogenetic stimulation at the soma (30 ms duration) and electrical field stimulation (EFS) of axon terminals to distal dendrites (0.1 ms duration). **b,** Kymographs (ΔF/F) along the red line in (**a**) comparing the effects of optogenetically triggered bAPs, EFS-triggered synaptic inputs, and both. Traces taken from the regions indicated by the colored arrows. **c,** Top: Fluorescence in a distal dendrite (> 200 µm) in response to combinations of optogenetic (30 ms, 3 bAPs, 1 dSpike) and EFS stimulation at various time offsets (ΔTime). Bottom: Corresponding data using 10 ms optogenetic

stimulation (1 bAP, 0 dSpikes). **d,** Area under the curve (AUC) for combined stimulus normalized to the sum of AUC for optical and EFS stimuli alone (*n* = 28 cells from 12 animals). **e,** AUC for combined stimulus as a function of ∆Time. Data for each cell scaled to the range [0, 1] (*n* = 8 cells from 7 animals for 30 ms stimulus; *n* = 5 cells from 4 animals for 10 ms stimulus). Open symbols represent individual data and filled symbols represent mean at each ∆Time. Red lines: exponential fit from -245 to 0 ms; sigmoidal fit from 0 to +245 ms. **f-g,** Sensitivity to D-AP5 (50 µM, *n* = 6 cells from 5 animals), TTX (20 nM, *n* = 4 cells from 3 animals), and $Ni^{2+}$ (100 µM, *n* = 4 cells from 4 animals) compared to the vehicle control (*n* = 11 cells from 8 animals). Sample traces overlaid with the baseline trace (gray). Box plots show median, $25^{th}$ and $75^{th}$ percentiles, and extrema. ***$p < 0.001$ vs. control, one-way ANOVA with Bonferroni's *post hoc* test. **h.** Schematic model showing how dendritic filtering of broadly distributed dSpikes combines with localized glutamate signals to activate NMDARs in synapses which contributed to an increase in spike rate.

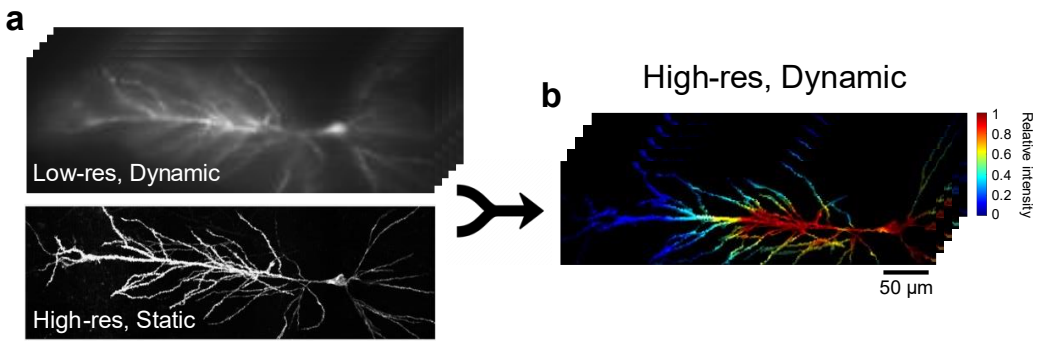


**Fig. S1 | Combining 1P and 2P images. a,** Low spatial-resolution, high-speed (1 kHz) recordings were acquired separately from high spatial-resolution static image (2P). **b,** The datasets were combined to produce high-resolution dynamic data. Related to Fig. 1.

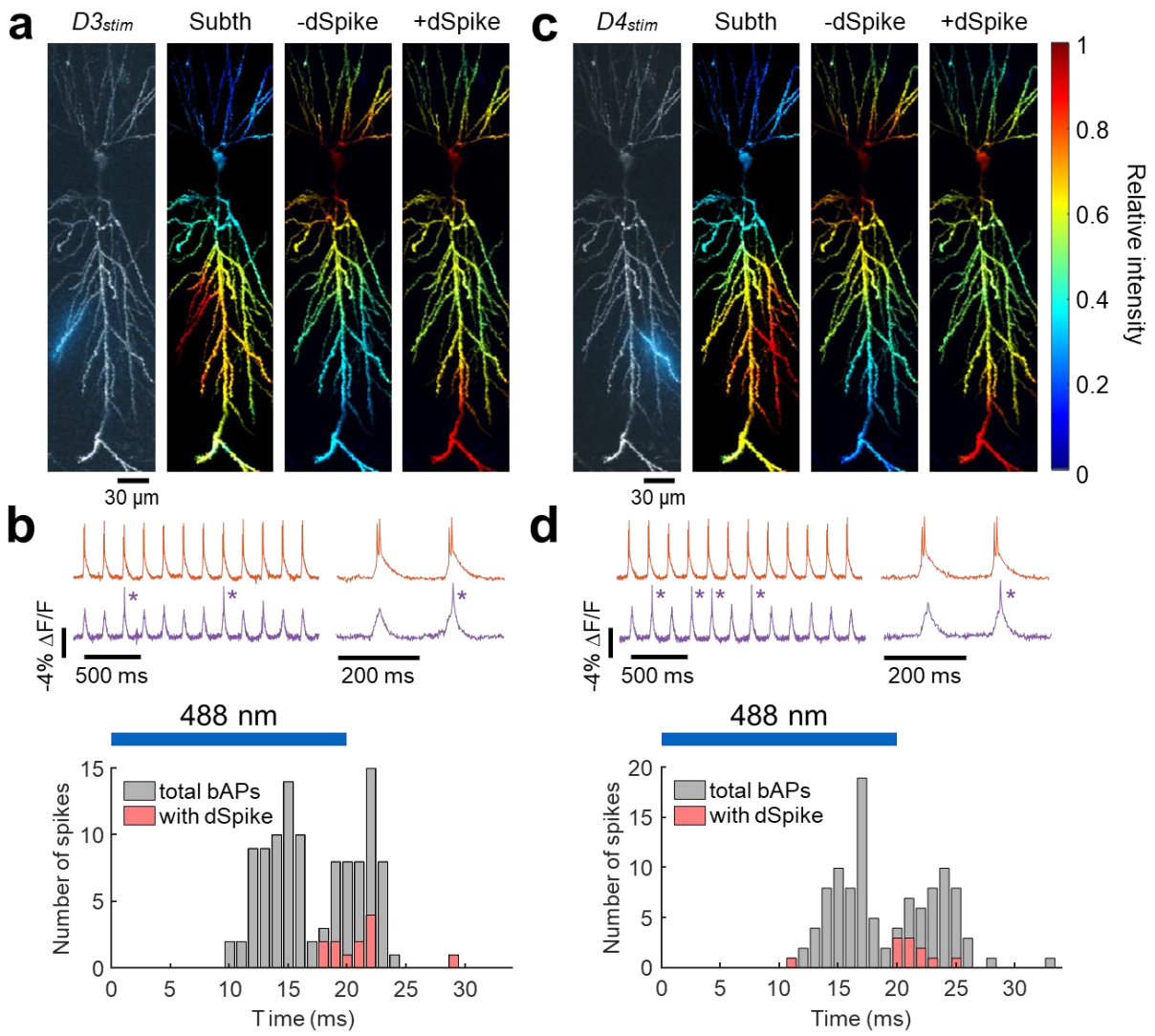


**Fig. S2 | Additional examples of responses to dendrite-targeted stimuli. a,** 2P structural image (gray) combined with the optogenetically stimulated region (blue; 20 ms duration, 5 Hz). Normalized amplitude ($\Delta F/F_{ref}$) maps for subthreshold depolarization (stimulus-triggered average from 54 trials), back-propagating action potentials (bAPs) without dSpikes (-dSpikes; spike-triggered average from 80 spikes) and with dSpikes (+dSpikes; spike-triggered average from 12 spikes). **b,** Top: example traces at the soma (orange) and distal dendrites (> 300 µm; purple) showing cases with dSpike (indicated by asterisk). Bottom: counting all bAPs, and bAPs with dSpikes, as a function of time following the optogenetic stimulation onset. Blue bar shows the timing of 488 nm (20 ms). **c-d,** Equivalent plots by stimulating a different dendrite ($D4_{stim}$; 54 trials, 85 -dSpikes, and 11 +dSpikes). Related to Fig. 2.

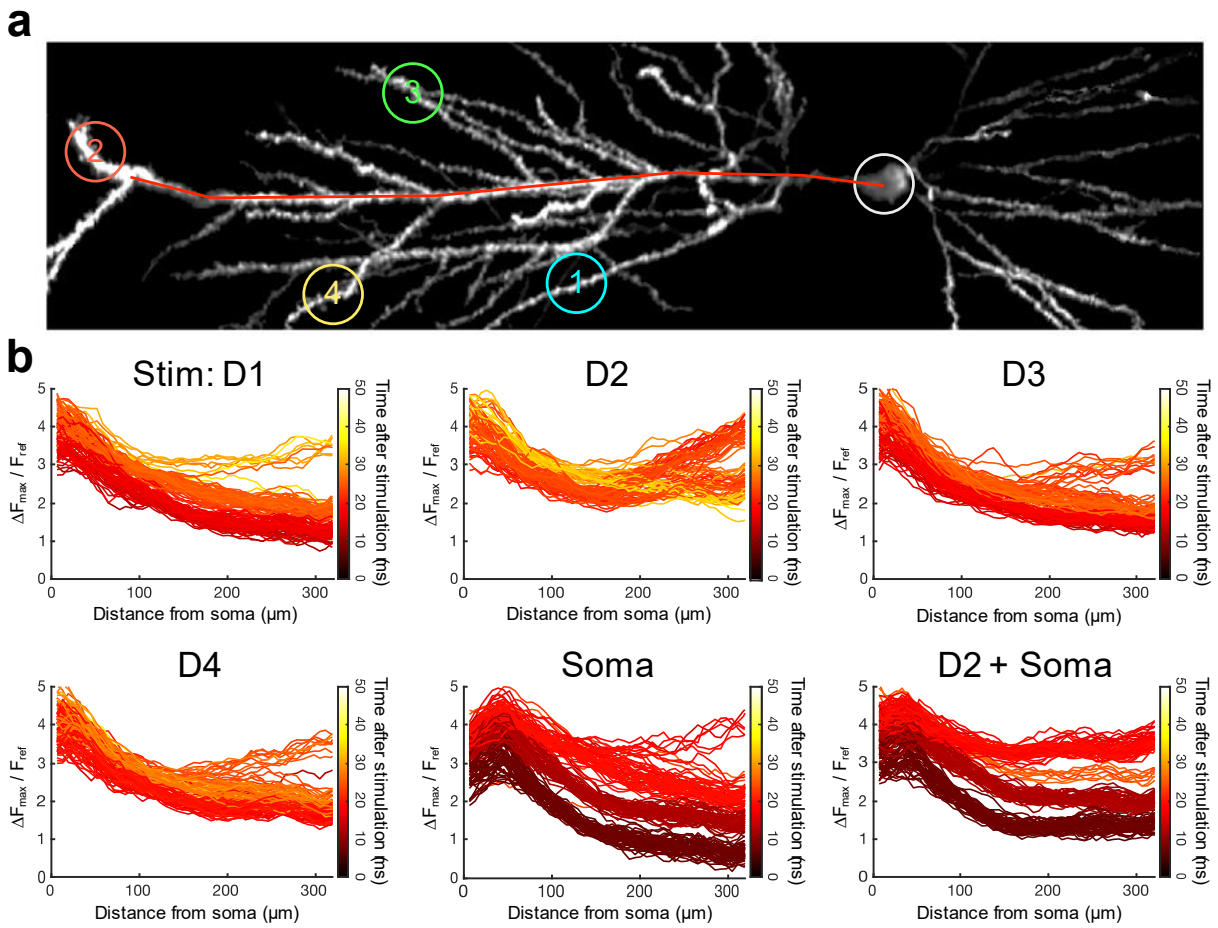


**Fig. S3 | Spatial profiles for individual bAPs. a,** 2P structural image (gray) showing stimulated branches indicated by numbers (20 ms duration at 5 Hz). **b,** Amplitude profiles for each bAP along the red line in (**a**). Plots were color-coded by the time after stimulus onset. Related to Fig. 2 and Fig. S2.

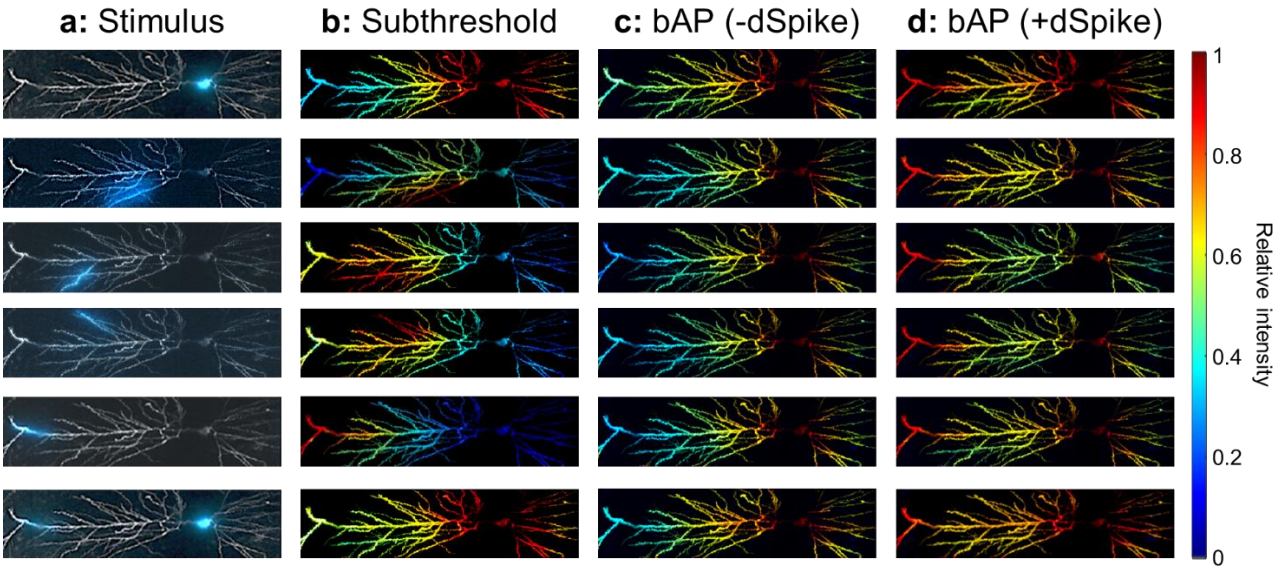


**Fig. S4 | Comparison of spatial maps for different stimulus locations. a,** 2P structural images (gray) combined with the optogenetically stimulated region (blue; 20 ms duration at 5 Hz). Normalized amplitude ($\Delta F/F_{ref}$) maps for **b,** subthreshold depolarization, **c,** back-propagating action potentials (bAPs) without dSpikes (-dSpikes) and **d,** bAPs with dSpikes (+dSpikes). Data from Fig. 2 and S2, arranged for side-by-side comparison.

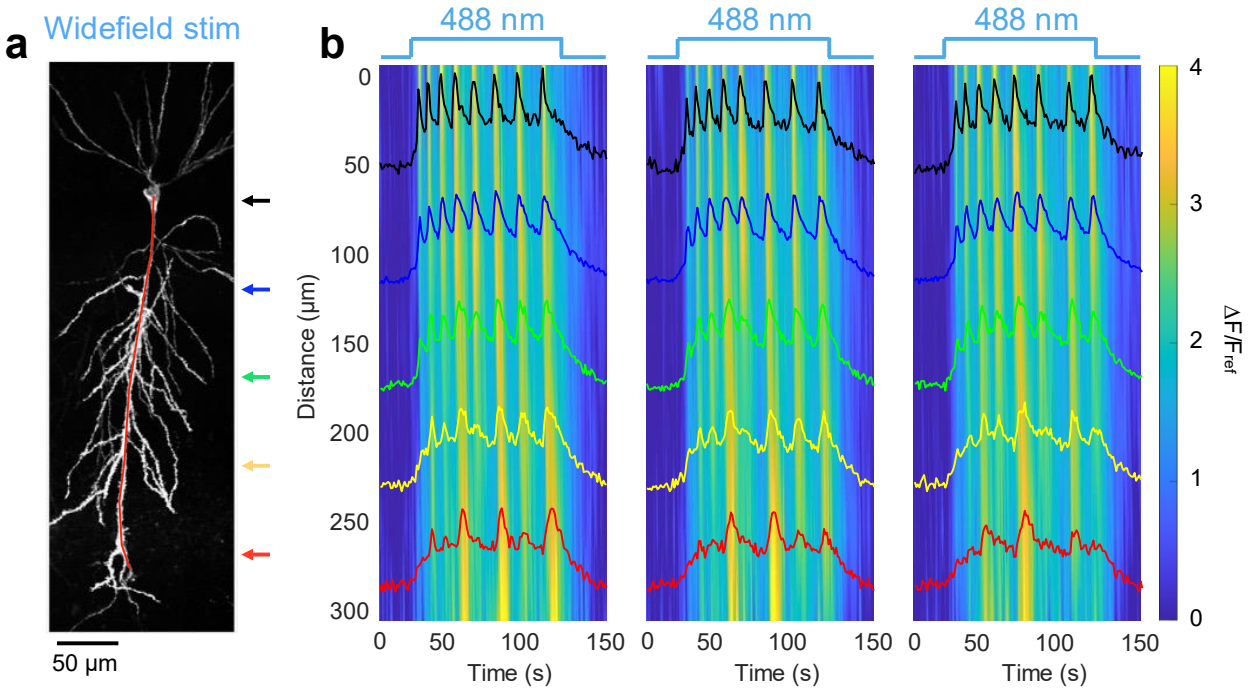


**Fig. S5 | Chaotic back-propagation. a,** 2P structural image showing the measured neuron. The cell was exposed to wide-field optogenetic stimulation (100 ms duration at 5 Hz). Red line indicates the backbone used to calculate a kymograph. **b,** Successive responses to pulses of blue light. The spike train in the soma was regular, but the pattern of bAP propagation showed trial-to-trial variability, indicative of chaotic back-propagation.

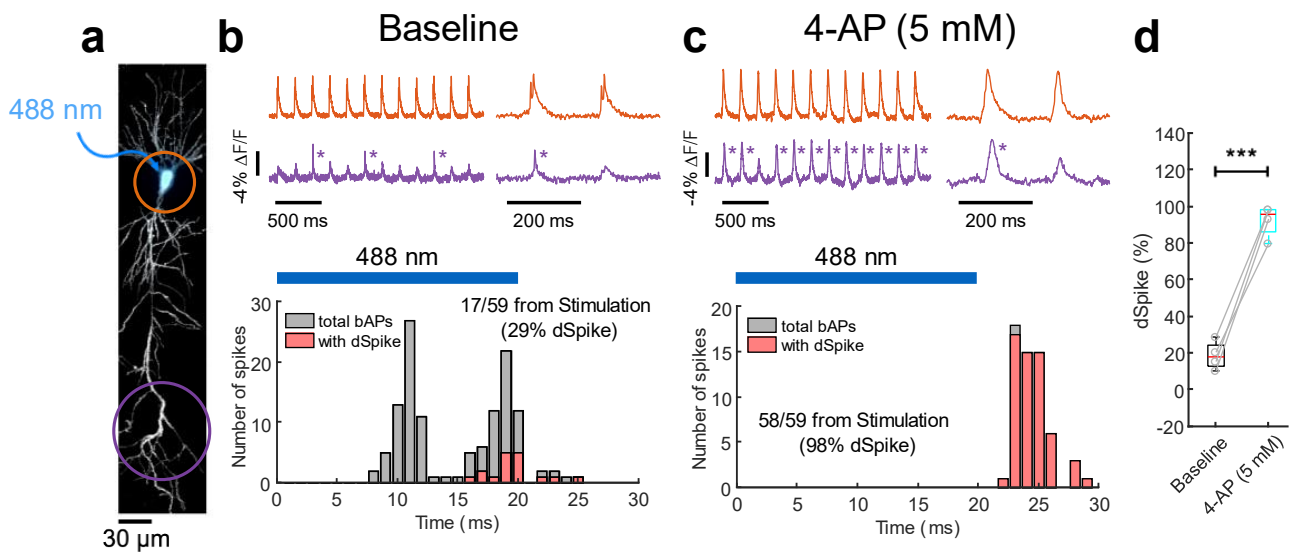


**Fig. S6 | dSpike sensitivity to 4-AP. a,** 2P structural image (gray) combined with the optogenetically stimulated region (blue; 20 ms duration at 5 Hz). **b,** Top: example traces at the soma (orange) and distal dendrites (> 300 µm; purple). DSpikes indicated by asterisks. Bottom: counting all bAPs, and bAPs with dSpikes, as a function of time following the optogenetic stimulation onset. Blue bar shows the timing of 488 nm (20 ms). **c,** Corresponding analysis for the same cell in the presence of 4-AP (5 mM) in the bath. **d,** Comparison of dSpike percentage for baseline vs. 4-AP (n = 4 cells from 3 animals). Box plots show median, 25$^{th}$ and 75$^{th}$ percentile, extrema. ***$p$ < 0.001, paired Student's t-test. Related to Fig. 3.

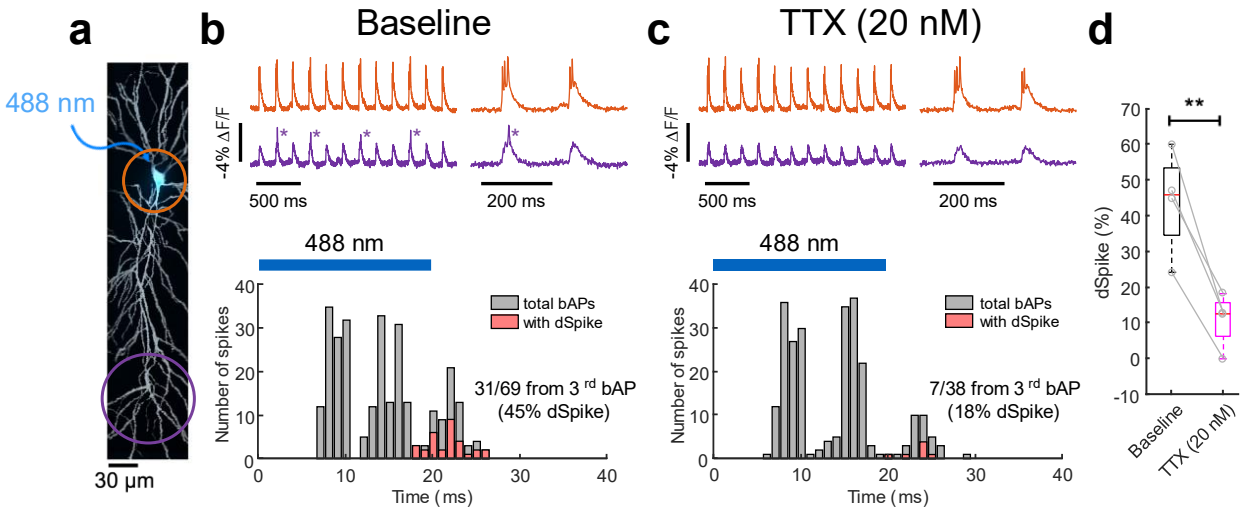


**Fig. S7 | dSpike sensitivity to low concentration of TTX. a,** 2P structural image (gray) combined with the optogenetically stimulated region (blue; 20 ms duration at 5 Hz). **b,** Top: example traces at the soma (orange) and a distal dendrite (> 300 µm; purple). DSpikes indicated by asterisks. Bottom: counting all bAPs, and bAPs with dSpikes, as a function of time following the optogenetic stimulation onset. Blue bar shows the timing of 488 nm (20 ms). **c,** Corresponding analysis in the presence of low concentration of TTX (20 nM) in the bath. **d,** Comparison of dSpike percentage for baseline vs. TTX (n = 4 cells from 3 animals). Box plots show median, 25$^{th}$ and 75$^{th}$ percentile, extrema. **$p$ < 0.01, paired Student's t-test. Related to Fig. 3.

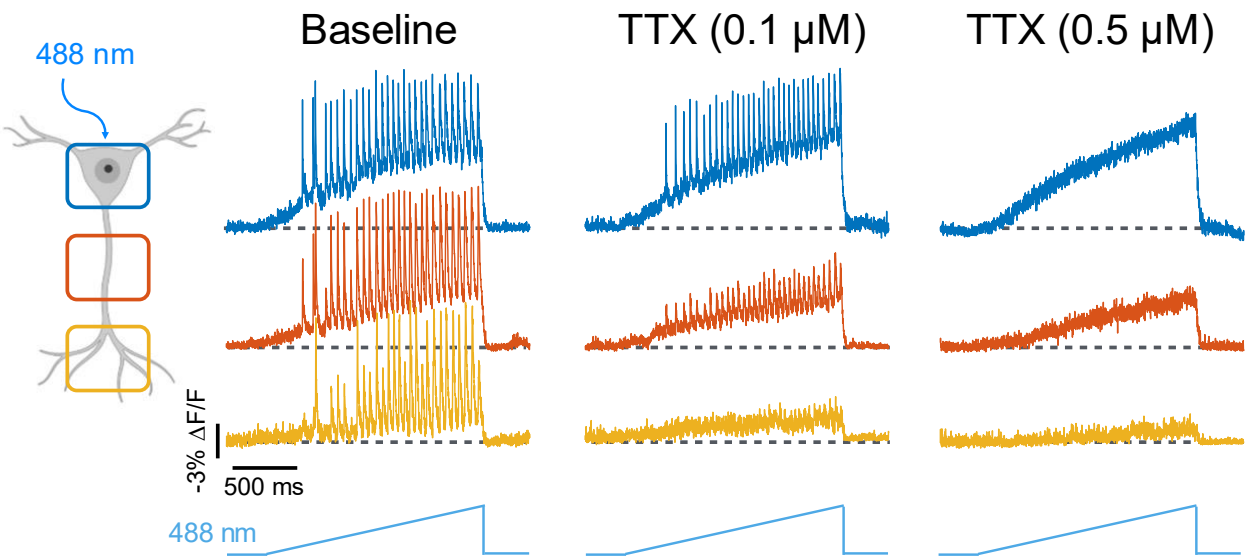


**Fig. S8 | Dose-dependent effect of TTX on dSpike formation.** Example neuron showing responses at the soma (blue), proximal (orange; < 200 µm from soma), and distal (yellow; > 300 µm) dendrites. Optogenetic stimulation was delivered to the soma using a gradually increasing ramp (2 s duration). The neuron was sequentially tested at 0.1 µM and 0.5 µM TTX in the bath using the same soma-targeted stimulus waveforms. At 0.1 µM, the soma continued to spike but dSpikes were suppressed. At 0.5 µM, spiking at the soma was suppressed. Related to Fig. 3.

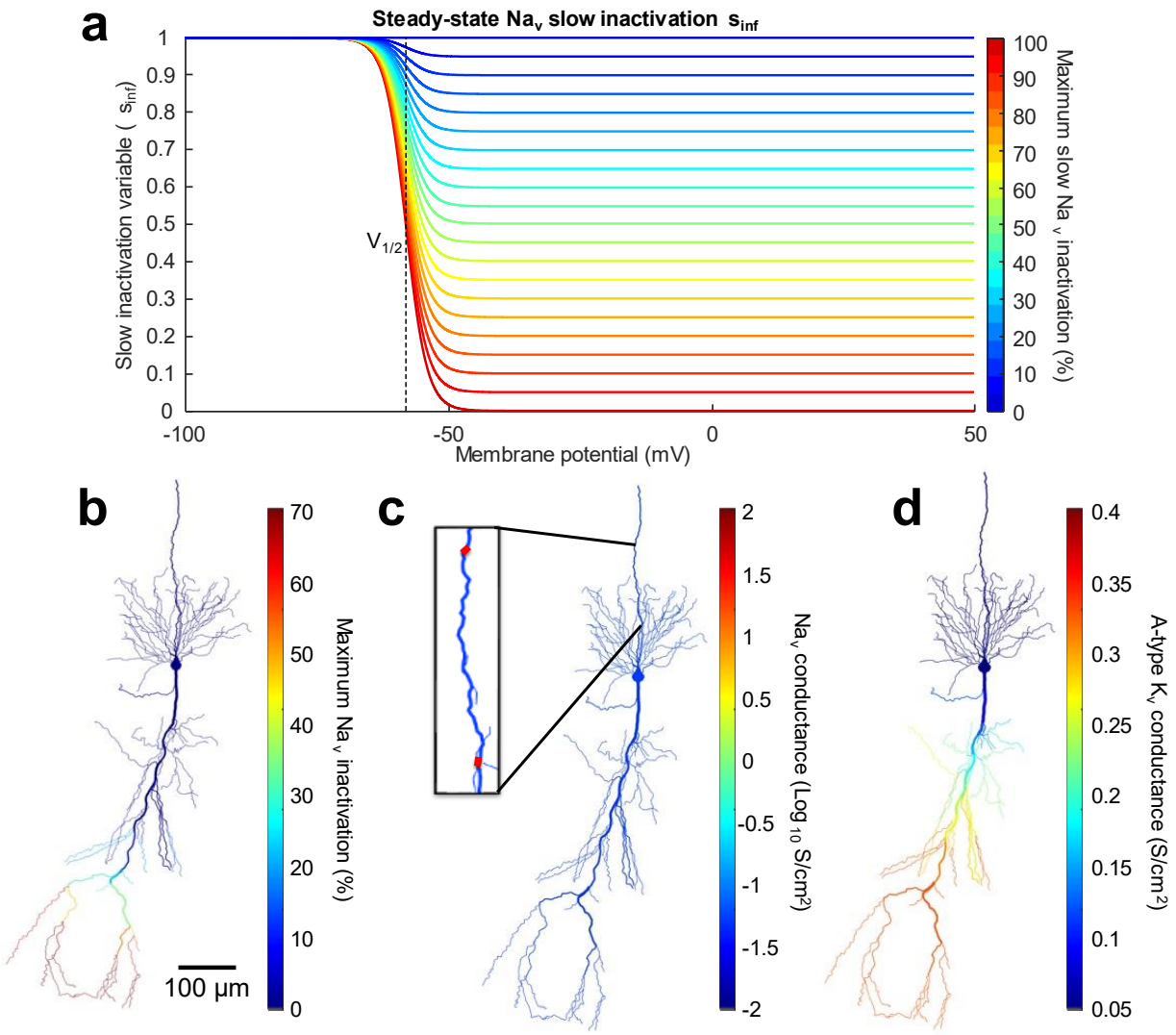


**Fig. S9 | Slow Na$_V$ inactivation and parameters for Na$_V$ and A-type K$^+$ channels in CA1 model.**

**a,** Voltage-dependent changes of slow Na$_V$ inactivation variables. Steady-state Na$_V$ inactivation is modeled as a mixture of inactivating and persistent currents as $s_{inf}(V, a_{r2}) = a_{r2} \cdot s_{inf}(V, 100\%) + (1 - a_{r2})$, where $a_{r2}$ is the proportion of inactivating channels and $s_{inf}$ (V, 100%) is the voltage dependent equilibrium value of the fully inactivating channels. **b,** Maximum Na$_V$ inactivation (%) across the neuronal compartments. **c,** Available Na$_V$ conductances distributed across the neuron ($g_{Na\,(max)}$), where $g_{Na} = g_{Na\,(max)} \cdot m^3 \cdot h \cdot s$ (m = channel activation variable; h = fast inactivation variable; s = slow inactivation variable). Note high density (30 S/cm$^2$) in nodes of Ranvier in the axon. **d,** Available A-type K$_V$ conductances distributed across the neuron ($g_{KA\,(max)}$), where $g_{KA} = g_{KA\,(max)} \cdot n \cdot l$ (n = channel activation variable; l = inactivation variable). Related to Fig. 3.

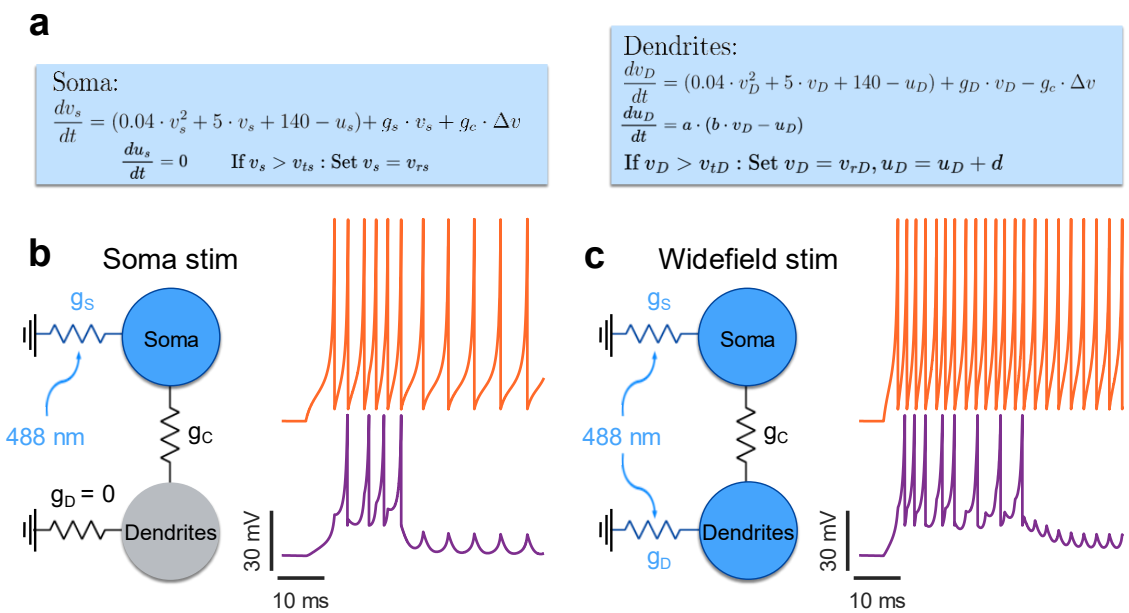


**Fig. S10 | Two-compartment Izhikevich model reproduces the dynamics of dSpike successes and failures. a,** Equations describing the two compartments. Soma without adaptation ($v_{ts}$ = 30, $v_{rs}$ = -55), dendrites with adaptation ($a$ = 0.0025, $b$ = 0.01, $d$ = 1, $v_{tD}$ = 0, $v_{rD}$ = -55). Coupling strength $g_c$ = 0.325. **b,** Soma only stimulation with $g_s$ = 0.16. Soma $v_s$ trace in orange, dendritic $v_D$ trace in purple. **c,** Combined somatic and dendritic stimulation with $g_s$ = 0.30, $g_D$ = 0.05. Soma $v_s$ trace in orange, dendritic $v_D$ trace in purple. Related to Fig. 3.

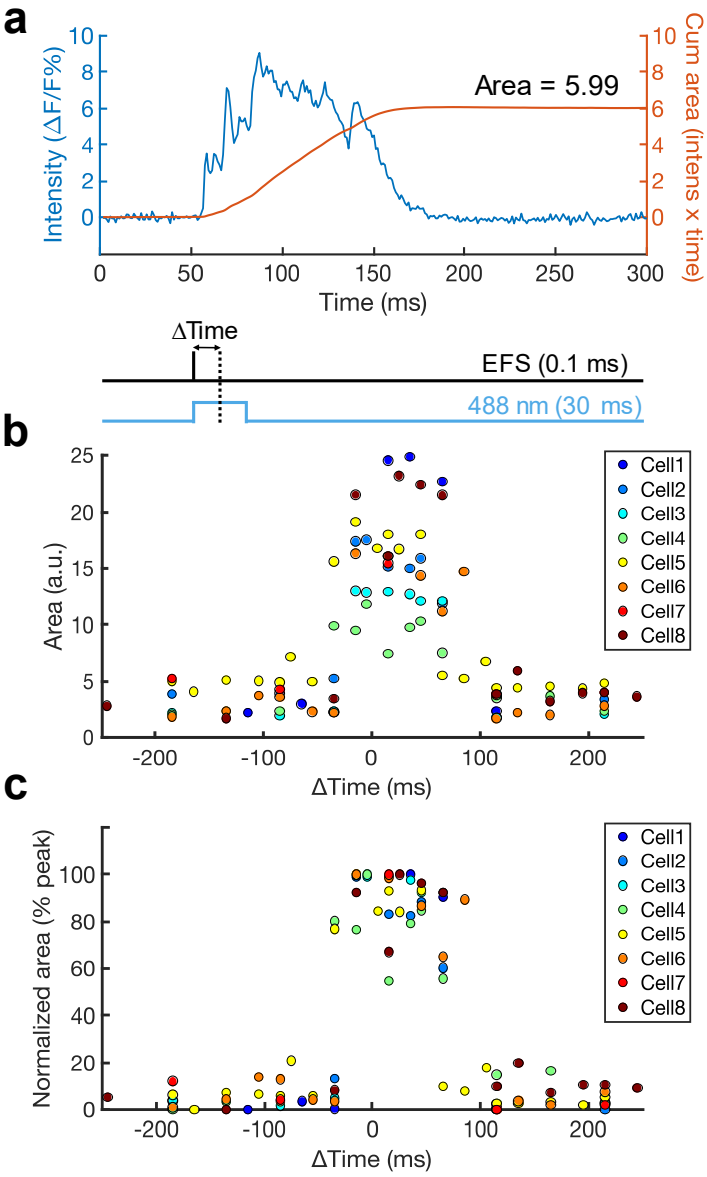


**Fig. S11 | Estimating areas of plateau potentials. a,** Example trace overlapped with cumulative area vs. time. **b,** Plateau areas vs. delay between EFS (0.1 ms duration) and optogenetic stimulation (488 nm, 30 ms at the soma). Each color represents a different cell. **c,** Normalized area with each cell mapped to the range [0, 1]. Related to Fig. 4.

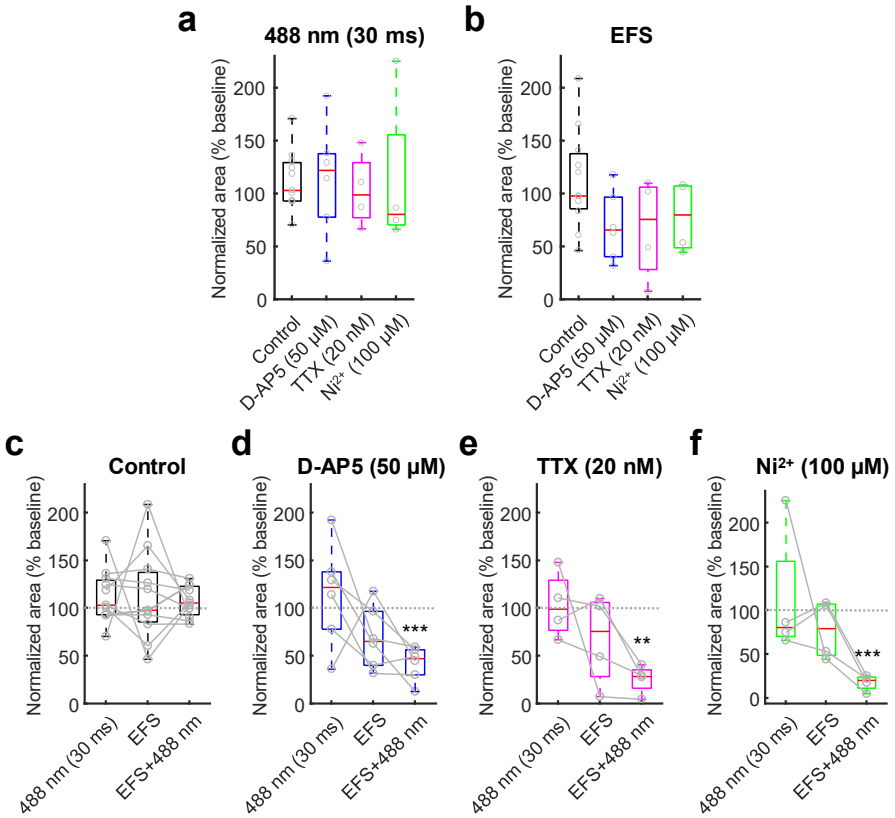


**Fig. S12 | Effects of channel blockers on EFS and optogenetic signals.** Effects of vehicle control ($n$ = 11 cells from 8 animals), D-AP5 (50 μM; $n$ = 6 cells from 5 animals), TTX (20 nM, $n$ = 4 cells from 3 animals), and $Ni^{2+}$ (100 μM, $n$ = 4 cells from 4 animals) on **a,** responses to optogenetic stimulation alone (30 ms at the soma), and **b,** responses to electric-field stimulation alone (EFS; 0.1 ms). Box plots show median, 25$^{th}$ and 75$^{th}$ percentiles, and extrema. Groups were compared by one-way ANOVA with Bonferroni's *post hoc* test. No significant difference observed between groups ($p$ > 0.05). **c-f,** Drug effects on the responses to optogenetic stimulation, EFS, and combined stimulation. Each condition was compared to each baseline by paired Student's t-test (*$p$ < 0.05, **$p$ < 0.01, and ***$p$ < 0.001 vs. baseline). Related to Fig. 4.